THERMODYNAMIC ANALYSIS OF HYDROGEN GENERATION

A Dissertation
Presented to
The Academic Faculty

By

Clarence Marcelle Buford

In Partial Fulfillment
Of the Requirements for the Degree
Doctor of Philosophy in Physics

Georgia Institute of Technology
November, 2003

THERMODYNAMIC ANALYSIS OF HYDROGEN GENERATION

Aproved by:

Dr. Robert. L Whetten

Dr. Phillip N. First

Dr. James Gole

Dr. Walter de Heer

Dr. Gary May

Date Approved: November 21, 2003

ACKNOWLEDGEMENTS

I would like to express my gratitude first to my undergraduate advisor, Dr. Abebe Kebede. Dr. Kebede noticed me amongst many other students in one of his physics lectures in 1993 at North Carolina A&T State University. He took an active roll in encouraging and supporting my academics. Because of his influence, I changed my major from electrical engineering to physics and I won a fellowship that funded my graduate school career.

I am grateful for Dr. James L. Smith who is a scientist at Los Alamos National Laboratory (LANL) and of whom I regard as an indispensable mentor. I had the pleasure of working with Dr. Smith as a summer research intern at LANL since 1994. Dr. Smith welcomed me and helped me to simplify many complexities of science research and of working with professionals.

My Mother, Clementine Buford, has served as a role model since I was a child. My mother worked tirelessly to send my brothers, sisters, and me to private school. She, being an educated woman, showed me through her life, the importance and power of education.

Lastly, my wife Tyra has been an unshakeable support to me for years and especially through the final and most difficult stages of my doctoral program. Thank you, Tyra, for enduring the hard times with me.

TABLE OF CONTENTS

LIST OF TABLES

LIST OF FIGURES

SUMMARY

Hydrogen is an energy carrier that can be used to create electricity via an electrochemical device called a fuel cell. Thus, many American scientists and policy makers consider hydrogen to be the fuel of the future because it can be produced without depending on petroleum imports. The research described in this dissertation investigates a thermodynamic model to predict results from and to compare methods of producing hydrogen.

Hydrogen generation will be explored through modeling two types of processes: steam reforming and supersonic pyrolysis. Results of the model predict that although methanol is a widely used fuel for steam reforming, dimethyl ether can produce the same amount of hydrogen when it is reformed while consuming less energy.

Supersonic pyrolysis is a well known process but has only recently been considered as a route to produce hydrogen. The model shows that pyrolysis could be a good alternative to steam reforming. Pyrolysis of fuels occurs at higher temperatures than does steam reforming and hence a higher energy input is necessary, however, hydrogen can be produced ten times faster making pyrolysis a more powerful method to produce hydrogen.

CHAPTER 1

INTRODUCTION

The object of the research described in this dissertation is to analyze "on-demand" hydrogen generation for fuel cell power applications in electric vehicles and electric appliances. Electricity can be created by the electrochemical process of a fuel cell.

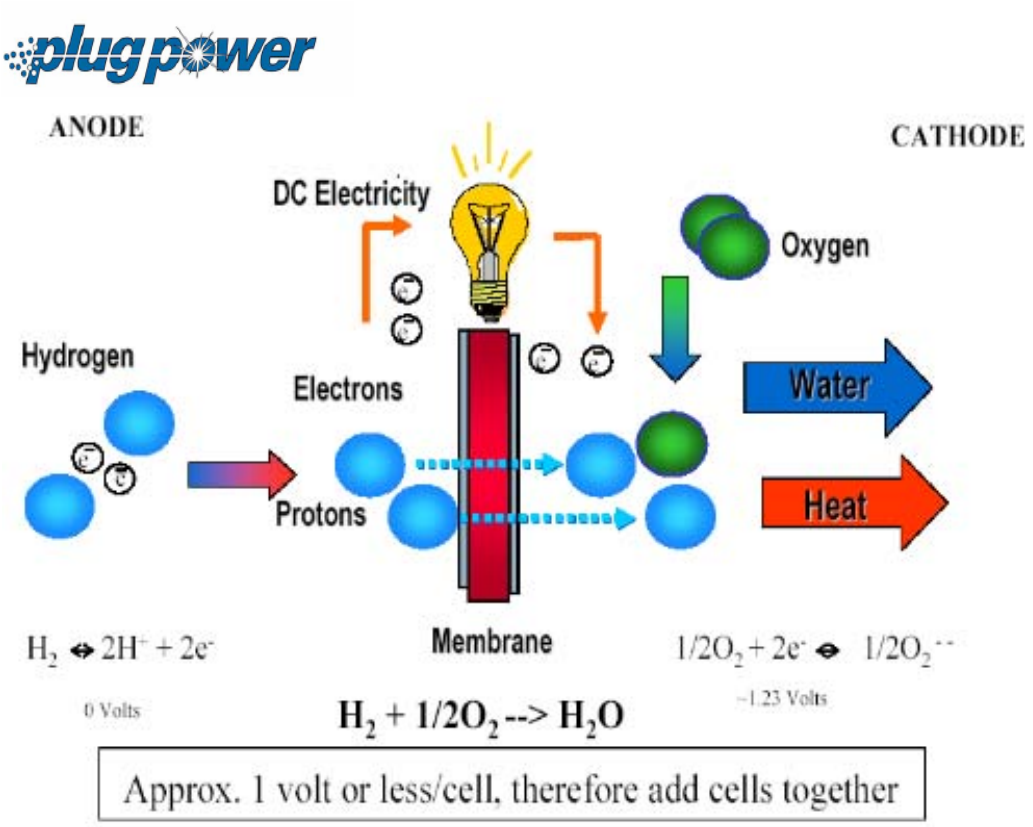

Figure 1. 1 Polymer electrolyte membrane fuel cell schematic. Hydrogen enters the anode side and oxygen enters the cathode. The hydrogen's protons can diffuse across the membrane to meet oxygen atoms. The hydrogen's electrons are shuttled across the electric load to provide power. Finally, hydrogen protons, electrons and oxygen atoms combine to create water.

Figure 1.1 is a schematic of a polymer electrolyte membrane fuel cell schematic. Hydrogen (H_2) can be generated by the reformation of alcohols, hydrocarbons, and other hydrogen containing molecules. Steam reforming is a simple chemical reaction between a hydrocarbon and steam yielding a carbon oxide and hydrogen. Numerical modeling techniques are employed to analyze suitability of reforming fuel mixtures for hydrogen generation processes, where the criteria are to maximize H_2 yield and minimize by-products of which carbon monoxide is the most undesirable. Two hydrogen generating processes will be modeled: steam reforming (SR) and supersonic pyrolysis. Fuels considered for steam reforming are methanol, methyl formate and dimethyl ether, while pyrolysis fuels are methane and ethane.

1.1 Environmental Concerns

Methanol is the most widely considered fuel for SR [1,2,3,4,5,6,7]. One of the serious concerns of using methanol as an alternative energy carrier is the potential for ground water contamination. Since methanol mixes readily with water, environmentalists fear that methanol spills will render water sources completely corrupt. Three types of methanol release scenarios have been evaluated by the U.S. Environmental Protection Agency (USEPA) [8]. Potential for accidental releases are considered from underground storage tanks, tanker trucks or rail cars, and ships or barges. Methanol is regarded as having an infinite miscibility in water thus, an accidental release into ground water or on the surface of an ocean would rapidly dilute to low concentrations (<1%). Plants and animals in the immediate vicinity of such spills would be impacted, however, once concentrations have been diluted to below toxic levels, methanol will biodegrade.

Biodegradation of methanol can occur under both aerobic (oxygen present) and anaerobic (oxygen absent) conditions by methylotrophs, organisms that ingest one-carbon compounds such as methanol and methane for use as their primary energy source [9]. Therefore, in any of the three release scenarios mentioned, methanol is not likely to persist in soil or water due to rapid dilution and biodegradation [10]. The very nature of methanol which environmentalists are most alarmed by, namely its miscibility in water, is precisely the mechanism that causes it to be benign.

1.2 Efficiencies

Theoretically, a perfect fuel cell has the same efficiency as a perfect Carnot heat engine. However, in practice, heat engines can not operate at their maximum combustion temperature because of the materials problems of handling the working fluid. Therefore, heat engines are forced to accept operating losses that fuel cells, operating at a much lower temperature can avoid [11]. If an electric vehicle is fueled by hydrogen gas (H_2FC), its drive train can operate with a mean efficiency of 47% compared to 18% for the internal combustion engine (ICEV) [12]. However, other factors affect the overall efficiency or the so called well to wheel efficiency (WTW). WTW includes the energy needed to recover and transport feed stock, fuel processing / refining, distribution and vehicle operation. All of these energy consuming steps need to be considered by decision makers to select fuels and drive trains that achieve the greatest energy benefits. It is also useful to divide WTW into two parts, well to pump (WTP) and pump to wheel (PTW) efficiencies. WTP is the efficiency up to the time of fueling a vehicle and PTW is the total fuel efficiency of a vehicle. The WTP for methane to hydrogen gas at 5000 psi is

73% and for crude oil to gasoline is 91% [13,14]. The PTW are 34% and 14% for the H_2FC and ICEV respectively. Taking the product of WTP and PTW gives 25% and 13% for WTW of H_2FC and ICEV respectively. A fuel cell vehicle with a methanol processing reformer on board (FCEV) attains a WTP of 72% for making methanol from methane. The FCEV operates at a PTW of 29% and has a WTW equaling 21%. Efficiencies are listed in table 1 for ease of comparison.

Table 1. 1 Well to pump (WTP), pump to wheel (PTW) and well to wheel (WTW) efficiencies for internal combustion engines (ICEV), Methanol reforming fuel cell (FCEV) and H_2 gas storing fuel cell vehicles (H_2FC)

	ICEV	FCEV	H_2FC
WTP	91%	72%	73%
PTW	14%	29%	34%
WTW	13%	21%	25%

Although, an H_2FC has an efficiency advantage, H_2 gas has low energy content. Storing liquid fuel "on board" for reforming will provide a dense fuel compared to storing pressurized gaseous H_2 in a vehicle. Liquid reforming fuels are a mixture of water and a fuel such as methanol. The water / fuel mixture may have a 1:1 molar ratio but are often 1.5:1 or 2:1. Consider an average automobile fuel tank having a volume of 12 gallon (US). If the water to methanol fuel feed has a unit molar ratio, the amount of the hydrogen produced from reforming this fuel can be calculated from equation 1.1. Reforming liquid fuel on board this vehicle results in 5.53 Kg of H_2 produced.

$$CH_3OH + H_2O \Leftrightarrow CO_2 + 3\ H_2 . \qquad (1.1)$$

If, in the same 12 gallon volume, gaseous hydrogen is pressurized to 5000 or 10,000 psi, the amount of stored hydrogen can be calculated using van der Waal's equation. In equation 1.2, P is pressure, a and b are van der Waal's constants for H_2, n is moles, V is volume, R is the ideal gas constant and T is temperature in degrees Kelvin. A mass of 0.985 Kg of H_2 will be stored in 12 gallons at 5000 psi and 1.55 Kg will be stored at 10,000 psi.

$$\left(P + a\frac{n^2}{V^2}\right) * (V - nb) = nRT \qquad (1.2)$$

There is more than a five-fold increase in the amount of H_2 stored in the liquid fuel when compared to a 5000 psi tank and more than three times the amount in the more dangerous 10,000 psi tank. The details are shown in Tables 1.2 and 1.3.

Table 1. 2 Mass of hydrogen produced from 12 gallons of methanol and water at ambient pressure.

	Methanol (CH_3OH)	Water (H_2O)	Hydrogen ($3H_2$)
Mass per mole	0.032 Kg	0.018 Kg	0.002 Kg
Density at 300K	$3.56\frac{Kg}{gal}$	$4.49\frac{Kg}{gal}$	4e-4 $\frac{Kg}{gal}$
Mass in 12 gal tank	29.48 Kg	16.6 Kg	5.53 Kg

Table 1. 3 Mass of H_2 stored in a 12 gallon fuel tank pressurized to 5000 and 10,000 psi at 300K

Pressure	a (atm L^2 mol^{-2})	b (L mol^{-1})	V (L)	moles of H_2	Mass of H_2
5000 psi	0.2476	0.0267	45.42	488.7	0.985 Kg
10,000 psi	0.2476	0.0267	45.42	767.5	1.55 Kg

In addition, with SR, water is a significant quantity of the fuel. Depending on the fuel mixture, water makes up 40% to as much as 70% of the fuel. Thus steam reforming can result in a 40-70% reduction of fossil fuel consumption in transportation.

These considerations illustrate why so-called "on-demand" hydrogen production from on-board liquid fuels is considered so attractive to many labs and industries. However, hydrogen production involves its own theoretical and technical challenges: it will not proceed to completion unless there is a strong thermodynamic driving force (ΔG), as determined by the reaction mixture composition, pressure, and electrochemical potential. Even when this condition is met, the hydrogen production rate may not be sufficient to match the need for H_2 consumption as provided by the fuel cell electro catalysts, so a catalyst is required. In this dissertation research, I have focused mainly on the former, thermodynamic criterion, as this has not been adequately described in the literature.

CHAPTER 2

THERMODYNAMIC CALCULATIONS

Chemical equilibrium in a reaction gas mixture is a dynamic process. A spontaneous approach toward equilibrium is observed when the initial partial pressures of the reactants are high and collisions between reactant molecules cause product molecules to form. Once the partial pressures of the products have increased sufficiently, the reverse reaction (forming "reactants" from "products") begins to occur. As the equilibrium state is approached, the forward and backward rates of reaction become equal and there is no further net change in reactant and product partial pressures [15]. The total Gibbs free energy function governs the forward and backward directions of chemical reactions. The composition at thermochemical equilibrium can be calculated by minimizing the Gibbs free energy, and so such equilibrium calculations provide a means to estimate the extent to which spontaneous chemical reactions will proceed. Equilibrium calculations provide a best-case effective-catalyst scenario for reaction dynamics without the need for complicated kinetic considerations. Some of the first uses of this method were in the area of rocket engine propellants and petrochemical processing [16,17]. Given the appropriate catalysts, a given reaction will proceed just as described by these calculations at reasonable speeds. A chemical reaction in a closed system, such as equation 1, can be thought of as consisting of M elements forming N constituents, where constituents are the reactants and products. Let A_i be the i^{th} constituent and n_i be the stoichiometric coefficient of the i^{th} constituent. Then,

$$\sum_{i}^{N} n_i A_i = 0. \qquad (2.1)$$

The stoichiometric coefficients of the products have positive signs and the reactants have negative signs; their absolute values are the number of moles of the i^{th} constituent. The premise of these thermodynamic calculations is to compute values of n_i for each constituent when the system equilibrates at a given temperature and pressure. A complete reaction converts all of the reactants to products at equilibrium thus, n_i equals zero for reactants. Knowing the value of $n_i(T,P)$ gives a measure of the completeness of the reaction. Since various temperature and pressure conditions are considered at equilibrium, the Gibbs free energy will be a very useful state function.

$$dG = VdP - SdT + \sum_{i=1}^{N} n_i \, d\mu_i \qquad (2.2)$$

At equilibrium, the Gibbs free energy is zero and, if equilibrium is achieved at constant temperature and pressure, then,

$$dG\big|_{T,P} = \sum_{i=1}^{N} n_i \, d\mu_i \qquad (2.3)$$

this can be called "materials equilibrium." Calculating the materials equilibrium is equivalent to finding n_i of our system such that the free energy is minimized. This is referred to as the non-stoichiometry formulation as the n_i's are not initially known. The function to be minimized is

$$G = \sum_{i=1}^{N} n_i \, \mu_i . \qquad (2.4)$$

But there is a constraint on the number of atoms in a particular reaction. If b_M is the number of atoms of element M in the reaction and a_M is the number of atoms of element M in constituent N. Then,

$$b_M = \sum_{i=1}^{N} a_{i,M}\, n_i \tag{2. 5}$$

describes the constraint. In order to minimize or maximize a function subject to a constraint, the Lagrangian multiplier method provides a swift solution. First, define a new function to be minimized such that

$$F = G + \varphi\, \lambda_M \tag{2. 6}$$

where

$$\varphi = \sum_{i=1}^{N} \left(a_{i,M}\, n_i\right) - b_M \tag{2. 7}$$

and λ_M is the Lagrangian multiplier.

$$F = \sum_{i=1}^{N} n_i\, \mu_i + \sum_{i=1}^{N} \lambda_M \left[\left(a_{i,M}\, n_i\right) - b_M\right] \tag{2. 8}$$

Following the Lagrangian multiplier methodology, F is differentiated with respect to n_i and with respect to the Lagrangian multiplier and both derivatives are equated to zero. Hence

$$\frac{dF}{dn_i} = 0 = \sum_{i=1}^{N} \left(\mu_i + \lambda_M\, a_{i,M}\right) \tag{2. 9}$$

$$\frac{dF}{d\lambda_M} = 0 = \sum_{i=1}^{N} \left(a_{i,M}\, n_i - b_M\right) \tag{2. 10}$$

Temperature and pressure dependence of equations 2.9 is found in μ_i. Since, from equation 2.4, the chemical potential is shown to be the Gibbs free energy per mole, μ_i has the same temperature and pressure dependence as G.

$$dG = VdP - SdT \tag{2. 11}$$

Then, holding the temperature constant, the free energy is

$$\int dG\big|_T = \int VdP \tag{2. 12}$$

Since the reactants and products are gases, the ideal gas law can be employed.

$$\int_{G^O}^{G} dG\big|_T = nRT \int_{P^O}^{P} \frac{dP}{P} \tag{2. 13}$$

$$G - G^O = nRT \ln\left(\frac{P}{P^O}\right) \tag{2. 14}$$

$$\mu - \mu^O = RT \ln\left(\frac{P}{P^O}\right) \tag{2. 15}$$

Where G^O, P^O and μ^O are the standard pressure values (at 1 bar) and G, P and μ are the values at the operating pressure. The chemical potential for a single constituent is

$$\mu_i = \mu_i^O + RT \ln\left(\frac{P_i}{P^O}\right) \tag{2. 16}$$

To obtain G as a function of the total pressure of the system, note that

$$P_i = xP \tag{2. 17}$$

and

$$x = \frac{n_i}{n} \tag{2. 18}$$

so that the chemical potential is now

$$\mu_i = \mu_i^O + RT\ln(P) + RT\ln\left(\frac{n_i}{n}\right) \tag{2. 19}$$

and the minimized functions become

$$\frac{dF}{dn_i} = 0 = \sum_{i=1}^{N}\left[\mu_i^O + RT\ln(P) + RT\ln\left(\frac{n_i}{n}\right) + \lambda_M\, a_{i,M}\right] \tag{2. 20}$$

$$\frac{dF}{d\lambda_M} = 0 = \sum_{i=1}^{N}\left(a_{i,M}\, n_i - b_M\right) \tag{2. 21}$$

In the non-stoichiometric formulation, the substances that can coexist in equilibrium must be previously defined [18]. A plot of the Gibbs free energy of formation, ΔG_f^O versus temperature, figure 2.1, provides an understanding of the compounds that are stable at a given temperature. Thermodynamics favor spontaneous formation of compounds that have low ΔG_f^O relative to others. Depending on the fuel compound with which a reaction starts, the ΔG_f^O plot reveals which stable compounds may form and what temperatures encourage their formation. From an understanding of thermodynamics through ΔG_f^O, appropriate compounds are inserted in to equilibrium calculations. The plot of ΔG_f^O is especially important to locate by-products. Important by products for steam reforming of methanol are carbon monoxide, unreacted methanol, and excess

steam. Methyl formate is also considered as a byproduct of methanol reforming, but calculations will show that it does not participate in the reaction.

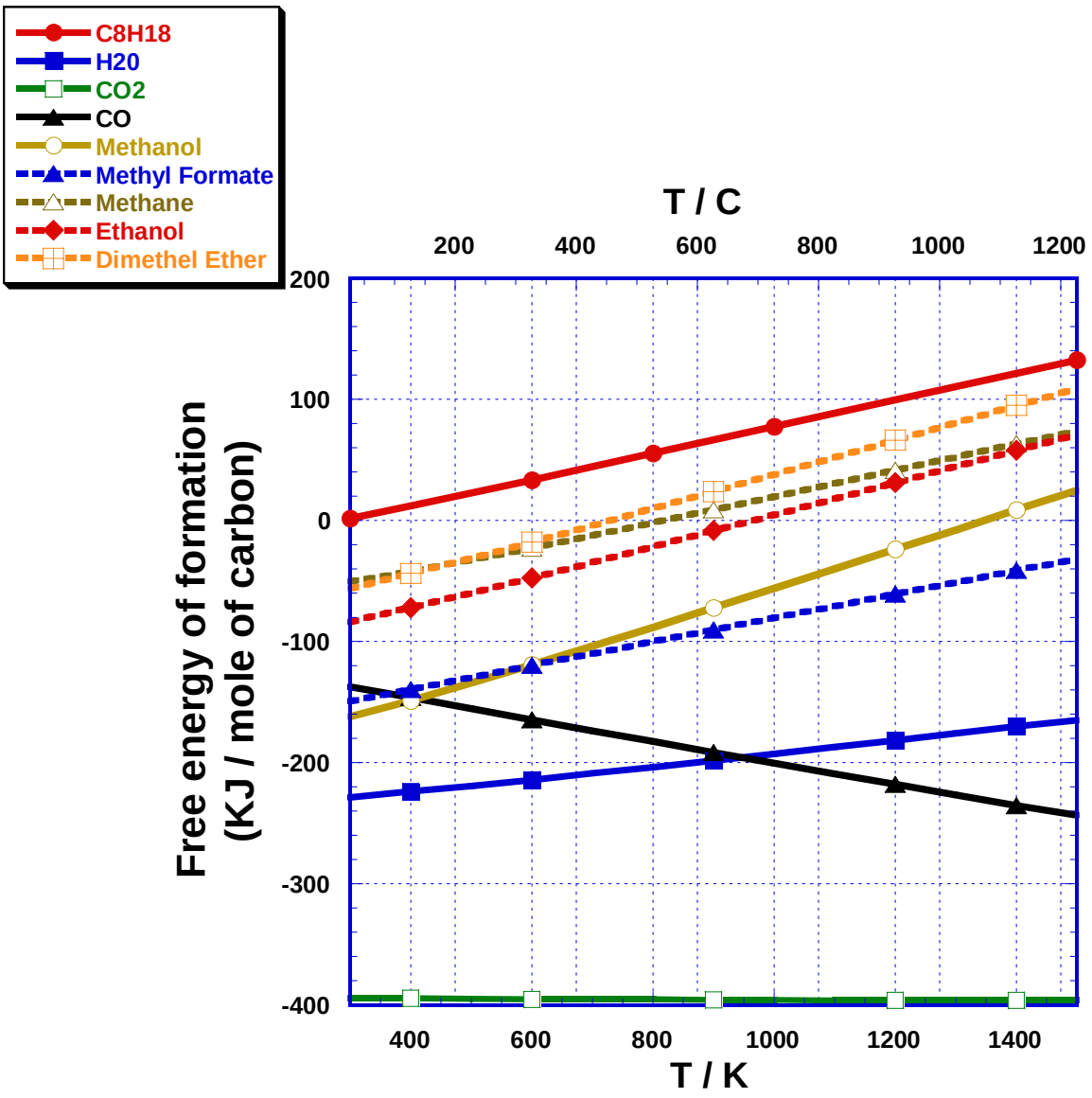

Figure 2.1 Free energy of formation (ΔG_f^o) at 1 bar and normalized for carbon content. SR products are given by those compounds whose ΔG_f^o is less than the compounds chosen to be the SR reactants.

There are N equations in the form of equation 20 and M in the form of 21. These equations are solved simultaneously yielding solutions for n_1 through n_6 for each constituent and by-product, for n_T and for $\lambda_C, \lambda_H, \lambda_O$. Below are the expanded forms of equation 20, 21 and an additional equation necessary to solve for n_T.

$$0 = \mu^{O}_{H_2} + RT\ln(P) + RT\ln\left(\frac{n_1}{n_T}\right) + 2\lambda_H + 0\lambda_C + 0\lambda_O \quad (2.\ 22)$$

$$0 = \mu^{O}_{H_2O} + RT\ln(P) + RT\ln\left(\frac{n_2}{n_T}\right) + 2\lambda_H + 0\lambda_C + \lambda_O \quad (2.\ 23)$$

$$0 = \mu^{O}_{CO_2} + RT\ln(P) + RT\ln\left(\frac{n_3}{n_T}\right) + 0\lambda_H + \lambda_C + 2\lambda_O \quad (2.\ 24)$$

$$0 = \mu^{O}_{CO} + RT\ln(P) + RT\ln\left(\frac{n_4}{n_T}\right) + 0\lambda_H + \lambda_C + \lambda_O \quad (2.\ 25)$$

$$0 = \mu^{O}_{CH_3OH} + RT\ln(P) + RT\ln\left(\frac{n_5}{n_T}\right) + 4\lambda_H + \lambda_C + \lambda_O \quad (2.\ 26)$$

$$0 = \mu^{O}_{CH_3OCHO} + RT\ln(P) + RT\ln\left(\frac{n_6}{n_T}\right) + 4\lambda_H + 2\lambda_C + 2\lambda_O \quad (2.\ 27)$$

$$0 = 2n_1 + 2n_2 + 4n_5 + 4n_6 - H \quad (2.\ 28)$$

$$0 = n_3 + n_4 + n_5 + 2n_6 - C \quad (2.\ 29)$$

$$0 = n_2 + 2n_3 + n_4 + n_5 + 2n_6 - O \quad (2.\ 30)$$

$$0 = n_1 + n_2 + n_3 + n_4 + n_5 + n_6 - n_T \quad (2.\ 31)$$

Computation of solutions to this system of algebraic non-linear equations is performed by a numerical algorithm from Numerical Algorithms Group's (NAG) `nag_nlin_sys FORTRAN module`. This module is based upon the MINPACK procedures HYBRJ and HYBRD [19]. Since the methods are iterative, an initial guess of the solution has to be supplied; the solution located will usually be the one closest to this initial guess. It is an iterative approximation to simultaneous solutions of algebraic non linear equations. This module chooses a correction at each step as a convex combination of the Newton and scaled gradient directions. The function nag_nlin_sys_sol is designed to solve a set of nonlinear equations in n unknowns as in equation 2.33.

$$f_i(x) = 0,\ i = 1, 2, \ldots, n,\ x = (x_1, x_2, \ldots, x_n)^T \qquad (2.\ 32)$$

It is assumed that the functions are continuous and differentiable so that the matrix of first partial derivatives of the functions, the Jacobian matrix $J_{ij}(x) = \partial f_i/\partial x_j$ evaluated at the point x, exists. The functions f_i must be independent, otherwise there will be an infinite number of solutions and the method will fail. The solution of a set of nonlinear equations can be regarded as a special case of the problem of finding a minimum of a sum of squares equation

$$s(x) = \sum_{i=1}^{r} [f_i(x_1, x_2, \ldots, x_s)]^2\ (r \geq s) \qquad (2.\ 33)$$

The procedure nag_nlin_sys_sol is provided for solving a set of nonlinear equations. This procedure requires the f_i to be calculated in user-supplied functions. The supplied functions are equations 2.22 – 2.31.

CHAPTER 3

EQUILIBRIUM ANALYSIS OF STEAM REFORMING FUELS

3.1 Introduction

Recall that steam reforming (SR) refers to a class of reactions in which a fuel molecule is oxidized, as in combustion, by the reduction of H_2O to H_2. Historically, these processes are the most important means of producing hydrogen. The fuels considered in SR are methanol (CH_3OH), methyl formate (CH_3OCHO) and dimethyl ether (CH_3OCH_3). The equations representing the complete SR of each fuel by excess H_2O are presented normalized for carbon. Thus, the equations for steam reforming of each fuel are as follows.

$$CH_3OH + x\ H_2O \Leftrightarrow (x-1)\ H_2O + CO_2 + 3\ H_2 \tag{3.1}$$

$$\tfrac{1}{2} CH_3OCHO + x\ H_2O \Leftrightarrow (x-1)\ H_2O + CO_2 + 2\ H_2 \tag{3.2}$$

$$\tfrac{1}{2} CH_3OCH_3 + x\ H_2O \Leftrightarrow \psi\ H_2O + \alpha\ CO + \beta\ CO_2 + \gamma\ H_2 \tag{3.3}$$

Besides temperature and pressure, the primary independent variable for SR is the quantity of steam introduced into the reaction. For each fuel composition, results will show the concentration of products as the molar quantity of steam is increased from 1 to 2.5 in steps of 0.5 moles and as temperature is increased from 300K to 1000K. Results will also show the generation of products measured in terms of mole fraction, mass fraction and moles. Mole fraction is the ratio of moles of a product to the sum of moles

of all products. Similarly, mass fraction is the ratio of the mass of a product to the mass of all products.

3.2 Methanol

Figures 3.1-3.4 are the plots of mole fraction of products from SR of methanol at 1 bar with increasing steam content or increasing the steam to carbon (S/C) ratio. Data plotted for temperatures less than the boiling point of water (373.15K) are usually regarded as not useful for analyzing steam reforming. The figures show that as steam becomes progressively more dominant in the influent, the factional amount of H_2 in the effluent decreases. The mole fraction has a dull apex around 400K that broadens with increasing steam in the feed gas.

It is not difficult to ascertain the cause of the enhancement of H_2 production with rising steam content. An inspection of the H_2O curves at 400K in figures 3.1-3.4 confirms that all of the excess steam entering the reaction leaves the reaction. For instance, figure 3.2 illustrates the composition of the effluent gas when there are 1.5 moles of steam in the feed gas. With x = 1.5 moles, in equation 1, the excess steam transferred to the product side should be 0.5 moles. At 400K, the mole fraction of H_2O is 0.1133 and since the total moles in the effluent is 4.5, the number of moles of H_2O is 0.5 which is exactly the amount of the excess. Hence, for methanol, the stoichiometric excess steam acts so as to drive the reaction to completion to produce more H_2 without participating in the reaction.

Conservation of the mass is illustrated by the H_2O and H_2 curves forming mirror images of each other. This mirror image becomes more discernable as the H_2O curve

approaches the H_2 curve with increasing steam in the feed. A similar mirror image can be observed between the CO_2 curve and the sum of the CO and CH_3OH curves. The number of moles in the reaction is constant, but the atoms of C, H and O are traded as certain molecules become more favorable at certain temperatures.

Figures 3.5- 3.8 are plots of mass fraction of H_2 produced with increasing steam in the feed gas. Mass fraction curves more truly represent the make up of the gas exiting a reformer. Mole fraction curves are useful to compare to chemical formulae, however, mass fractions are more intuitive. Carbon dioxide is a by-product of steam reforming which receives much attention owing to its touted "green house effect" on the earth's climate. Estimates given by climatologists put the yearly growth rate of CO_2 at 3% and project the year for doubling of the present amount to be 2065 AD[20]. Because of complex mechanisms which control both the terrestrial surface temperature and the CO_2 cycle, there is no general consensus between climatic models clarifying the magnitude of the greenhouse warming and the consequence of doubling atmospheric CO_2[21]. Nevertheless, it is prudent to give a detailed description of the generation of CO_2 caused by steam reforming.

CO_2 production is proportional to H_2 production. Maximizing H_2 will necessarily accompany a maximum in CO_2 generation. CO_2 production rises at low temperatures until all of the carbon converted from the methanol is used to form CO_2 through the water gas shift reaction and saturates when the reaction converts all of the carbon (1 mole) to CO_2. CO_2 production saturates only with excess steam in the fuel feed. CO_2 is the prevailing curve in each of mass fraction plots even with 2.5 moles of steam in the feed. Only at high temperatures, when CO is more favorable, does CO_2 not lead in the amount

of mass produced. It is important to note that though the mass fraction of CO_2 varies with temperature, at a given temperature the total mass of CO_2 is largely unaffected by increasing steam. A comparison of the CO_2 curves in figures 3.1-3.4 shows a consistent value in grams per each temperature. H_2 is the second largest mass produced at 400K for S/C = 1 and the third largest for S/C > 1. The mass fraction of H_2 falls from 11.7% in figure 3.5 to 7.8% in figure 3.8 and varies only slightly with temperature. However, the excess steam allows the reaction to improve H_2 production from 5.84 to 6.04g.

Figure 3.9 is a plot of the moles of H_2 produced versus temperature. The four curves in the plot show that the moles of H_2 increase with the increasing S/C ratio of the feed. The moles of H_2 produced asymptotically approach the stoichiometric maximum of three. The peak of the H_2 curve moves to lower temperatures as the S/C ratio is increased. The S/C = 1 curve peaks at 430K and the S/C = 2.5 curve peaks at 410K. The lowering of the curve peaks partially offsets the additional energy necessary to warm the excess steam to operating temperatures. From equation 3.5 and the following example calculation, it costs 68.5KJ to warm 1mole of water to 430K from room temperature. An additional 10KJ is needed to warm 2.5 moles of water to 410K from room temperature.

$$\Delta H = nC_p\Delta T \qquad (3.4)$$

$$\Delta H_1 = (1\text{mole})(76\ \text{J/mole K})(373.15\text{K}-298.15\text{K}) = 5.7\text{KJ}$$

$$\Delta H_2 = \Delta H\text{vap} = 61\text{KJ}$$

$$\Delta H_3 = (1\text{mole})(33.9\ \text{J/mole K})(430\text{K}-373.15\text{K}) = 1.9\text{KJ}$$

$$\Delta H = \Delta H_1 + \Delta H_2 + \Delta H_3 = 68.6\text{KJ}$$

Carbon monoxide is the most undesirable by-product because it rapidly deactivates the Pt-based anode catalyst [22,23] of the polymer electrolyte membrane fuel cell (PEMFC), figure 1.1, and thus deep removal of CO to the parts per million (ppm) level is necessary [24]. The anode catalyst of the PEMFC is poisoned by only 10-40ppm CO [25,26]. Figure 3.10 is a plot of CO in ppm. The CO curves were generated by multiplying by10,000 the CO mole fraction data. At the temperature of the peak in the H_2 curves, CO is listed for each S/C ratio in table 1. For CO levels greater than 40 ppm, CO oxidation reactors should be employed to convert CO to CO_2 [27]. Increasing the amount of steam in the fuel feed reduces the amount of CO of the reformate by the same process that increases the amount of H_2. The water gas shift reaction diminishes CO by oxidizing it to CO_2 Figure 3.10 shows that the maximum tolerable amounts of CO are pushed to high temperatures as steam is increased. This trend is also expected to continue until amounts of CO are untraceable at extremely high temperatures.

Equilibrium calculations were taken at 1, 10 and 20 bar to determine the pressure dependence of SR (not shown). Hydrogen production is affected by pressure as expected by Le Chatelier's principle. Le Chatelier's principle states that a system in equilibrium that is subject to a stress will react in a way that counteracts the stress. Since the products of steam reforming of methanol are the gaseous molecules of carbon dioxide, water and hydrogen, these will increase the pressure of the reaction chamber container. Increasing the ambient pressure of the reaction chamber to 10 or 20 bar subjects the reforming reaction to a stress that it is obliged to counteract according to Le Chatelier's principle. The reforming products show a sharp decline to offset the pressure on the system. At 400K, H_2 production at 10 bar is 83% of its value at 1 bar, at 20 bar is only 70%.

Table 3.1 CO content of methanol reformate gas at temperature of maximum H_2 production

	CO (ppm)	T (K)
S/C = 1	151	430
S/C = 1.5	13	416
S/C = 2	5.3	412
S/C = 2.5	3.6	410

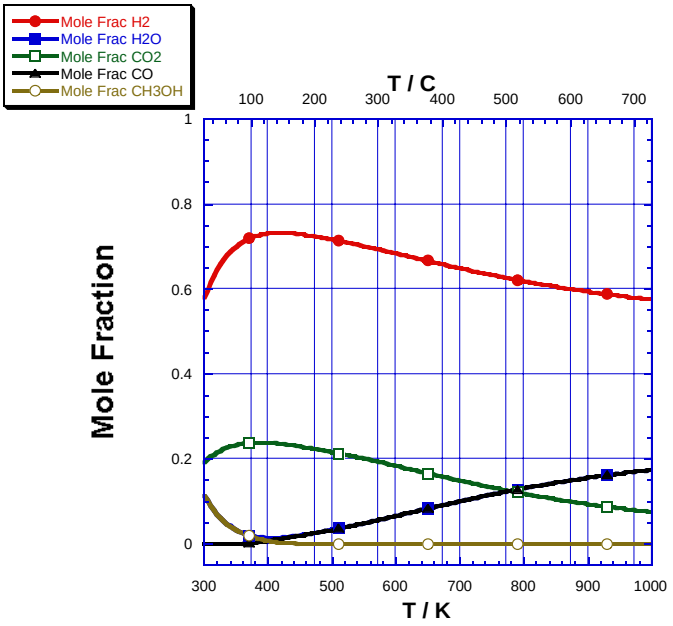

Figure 3. 1 Mole fraction of methanol products at 1 bar and S/C = 1. As steam becomes progressively more dominant in the influent, the factional amount of H_2 in the effluent decreases.

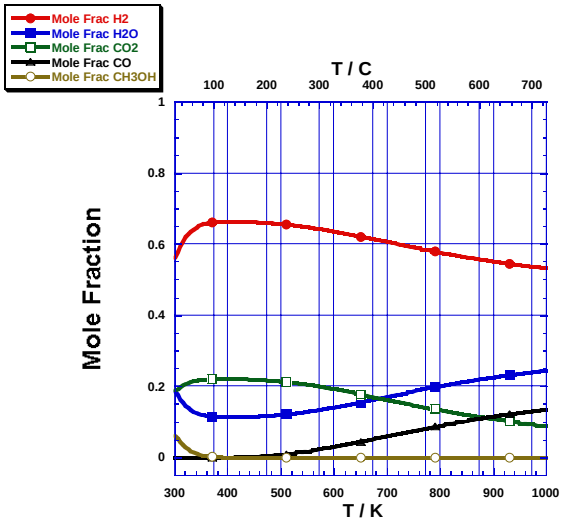

Figure 3. 2 Mole fraction of methanol products at 1 bar and S/C = 1.5. All of the excess steam entering the reaction leaves unreacted.

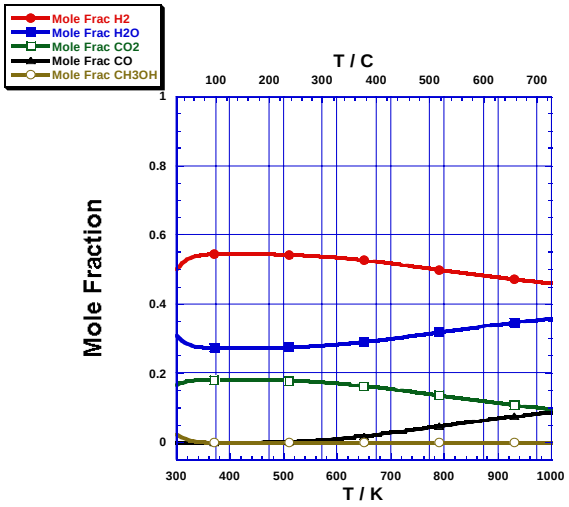

Figure 3. 4 Mole fraction of methanol products at 1 bar and S/C = 2.5

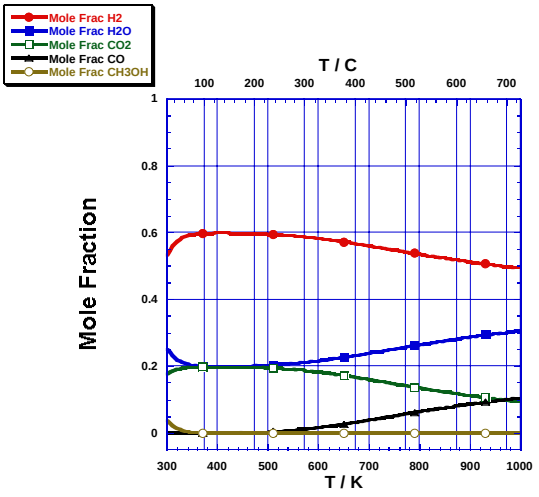

Figure 3. 3 Mole fraction of methanol products at 1 bar and S/C = 2. A dull apex around 400K broadens with increasing steam in the feed gas.

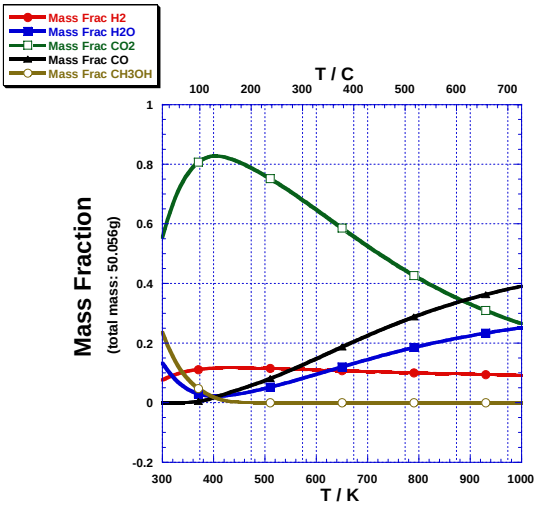

Figure 3. 5 Mass fraction of methanol products at 1 bar and S/C = 1. CO_2 production is proportional to H_2 production. Maximizing H_2 will necessarily accompany a maximum in CO_2 generation.

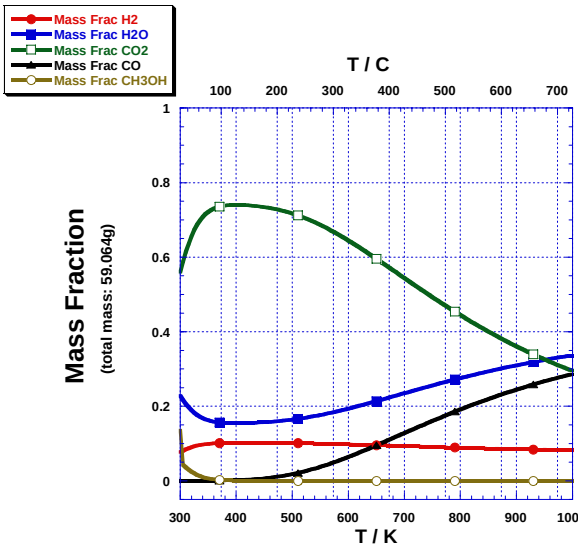

Figure 3. 6 Mass fraction of methanol products at 1 bar and S/C = 1.5. CO_2 production rises at low temperatures until all of the carbon converted from the methanol is used to form CO_2 through the water gas shift reaction.

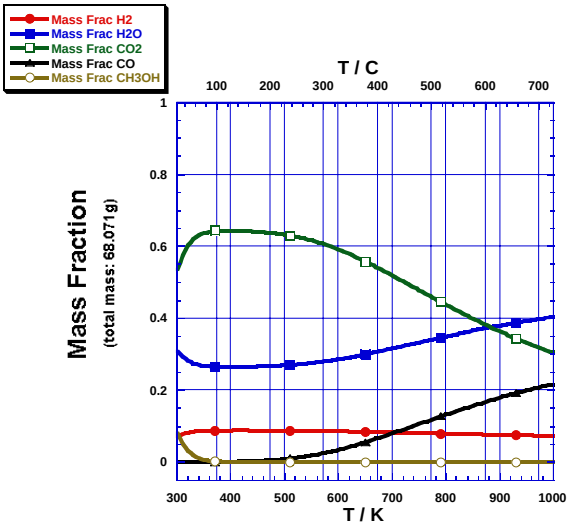

Figure 3. 7 Mass fraction of methanol products at 1 bar and S/C = 2. The mass fraction of H_2 falls from 11.7% in figure 3.5 to 7.8% in figure 3.8 and varies only slightly with temperature. However, the excess steam allows the reaction to improve H_2 production from 5.84 to 6.04g

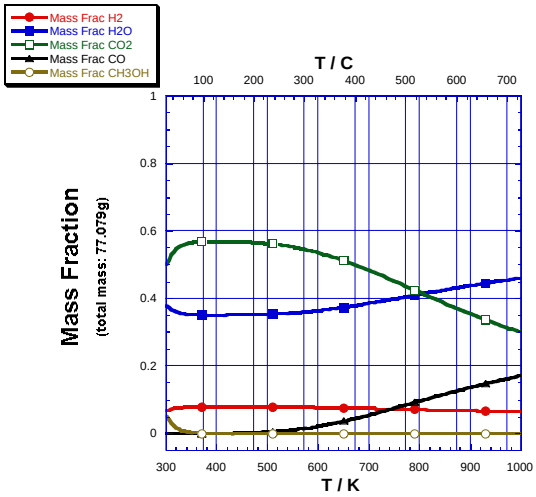

Figure 3. 8 Mass fraction of methanol products at 1 bar and S /C = 2.5. CO_2 production reaches the maximum stoichiometric amount only with excess steam in the fuel feed. CO_2 is the prevailing curve in each of the mass fraction plots even with 2.5 moles of steam in the feed.

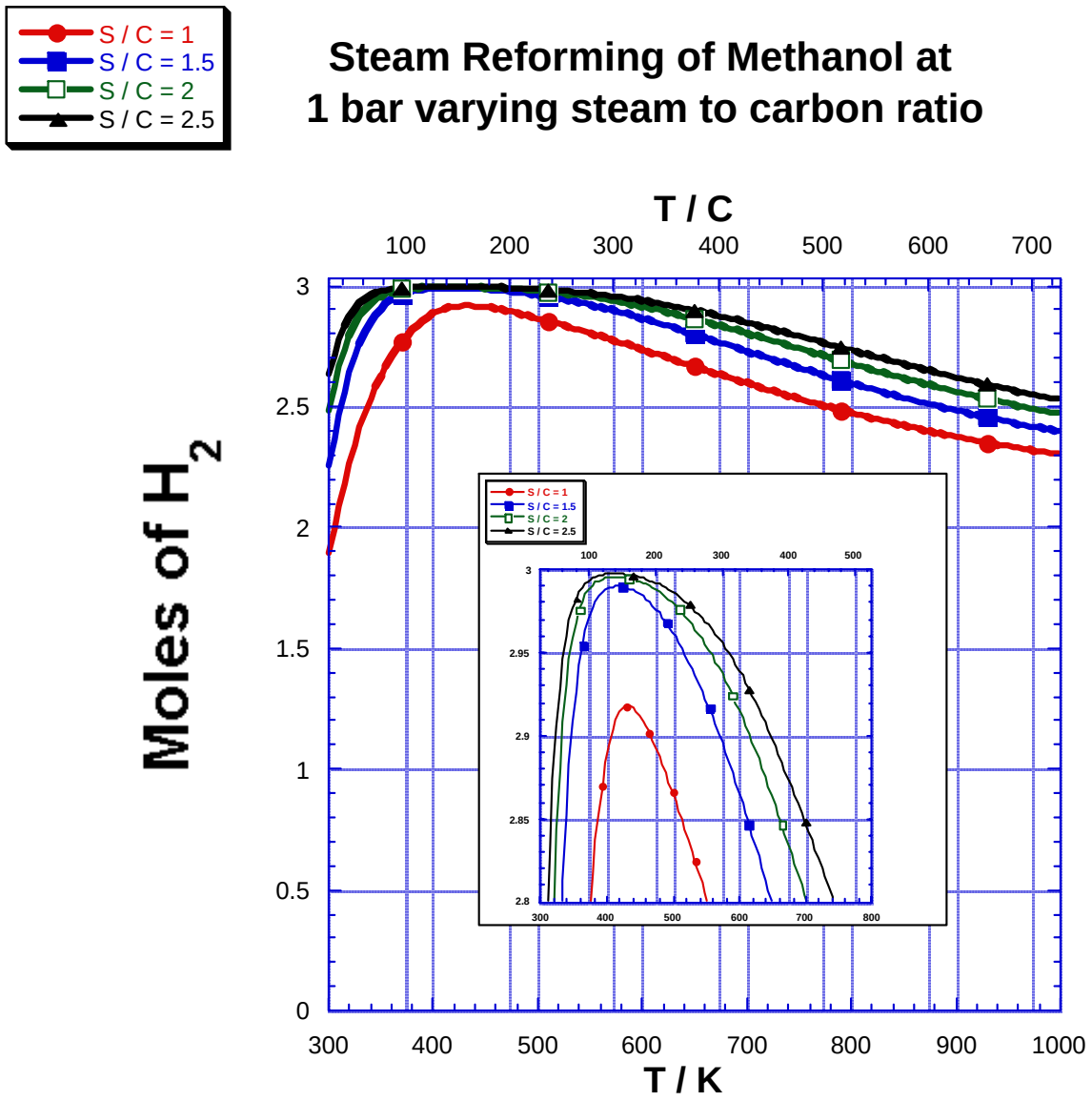

Figure 3. 9 Moles of H_2 produced from steam reforming of methanol at 1 bar varying steam to carbon ratio. The four curves in the plot show that the moles of H_2 increases with increasing the S/C ratio of the feed. The moles of H_2 produced asymptotically approaches the stoichiometric maximum of three.

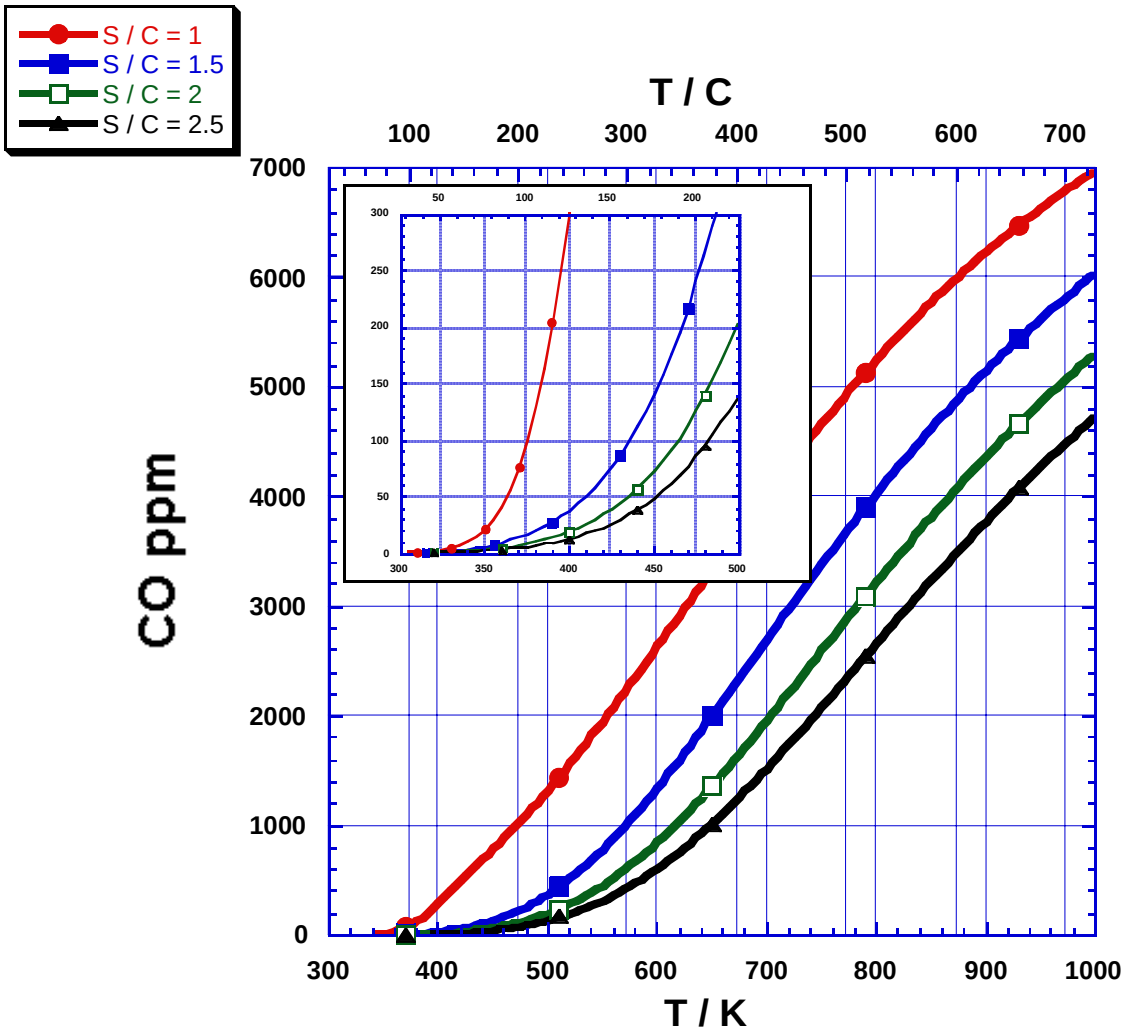

Figure 3. 20 CO production from steam reforming of methanol at 1 bar varying the steam to carbon ratio. At the temperature of the peak in the H_2 curves, CO concentrations are listed for each S/C ratio in table 1.

3.3 Methyl Formate

Methyl formate is included as a fuel for steam reforming because its reaction with steam is less endothermic than is methanol's. Hence, the reaction of equation 3.2 will require a smaller contribution from external energy sources to keep the fuel at required temperatures. The change in the enthalpy of reaction (ΔH_r) is negative for exothermic reactions and positive for endothermic reactions. ΔH_r is calculated at a specified temperature by summing the enthalpy of formation of reactants and subtracting that quantity from sum of the enthalpy of formation of the product molecules. At 400K, ΔH_r of equations 3.1 and 3.2 are 52.9KJ and 24.88KJ respectively. Then, ΔH_r per mole of H_2 produced is 17.63 KJ for methanol and only 12.44 KJ for methyl formate**.** Note that as excess steam is added, reforming reactions become more endothermic and thus require more energy from external sources to warm reactants to operating temperatures. In addition, methyl formate has a lower flash point than methanol, -19 °C and 11 °C respectively making it more reactive and more quickly brought to operating temperatures.

Figures 3.11-3.14 are the mole fraction plots for methyl formate reforming. These curves are nearly identical in shape to the methanol mole fraction curves. The H_2 mole fraction curves peak at close to 400K but unlike methanol, the fractional amount is lower. Figures 3.15-3.18 are the mass fraction plots from steam reforming of methyl formate. CO_2 again dominates the mass fraction plots at approximately 80% for S/C = 1 and 1.5 and approximately 60% for S/C = 2 and 2.5. As with methanol, the fraction of CO_2 decreases as the S/C ratio increases. Since CO_2 content is saturated, the additional mass of excess steam tends to decrease the fraction of CO_2 and all other constituents.

Figure 3.19 is the plot of H_2 moles produced from reforming of methyl formate. The H_2 curves show the characteristic rise and shift to lower temperatures of the peaks with increased S/C. Resembling methanol, these curves also display a substantial broadening of their maximum values and lengthening of the range of operating temperatures. A peak plateau can be defined for the range of temperatures that cover 99% of the peak value of H_2 moles produced. Thus the S/C = 1 plateau ranges from 400-408K, the S/C = 1.5 plateau range from 373.15-500K and the S/C = 2 and 2.5 plateaus ranges from 373.15-560K. Figure 3.20 is the plot of CO produced from steam reforming of methyl formate and table 3.2 provide supplementary details.

Table 3. 2 CO content of methyl formate reformate gas at temperature of maximum H_2 production

	CO (ppm)	T (K)
S/C = 1	153	428
S/C = 1.5	9.8	411
S/C = 2	3.9	407
S/C = 2.5	2.1	405

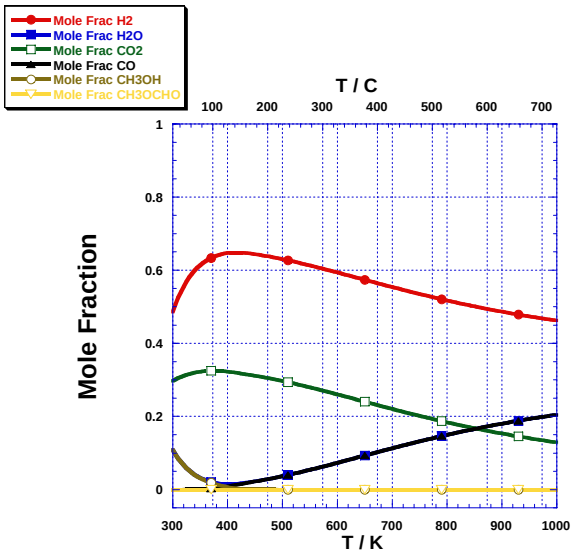

Figure 3. 11 Mole fraction of methyl formate products at 1 bar and S/C = 1. These curves are nearly identical in shape to the methanol mole fraction curves. The H_2 mole fraction curves peak at close to 400K but unlike methanol, the fractional amount is lower.

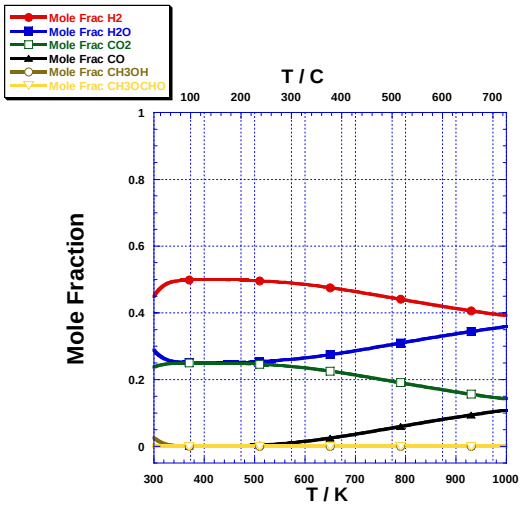

Figure 3. 13 Mole fraction of products from steam reforming of methyl formate at 1 bar and S/C = 2

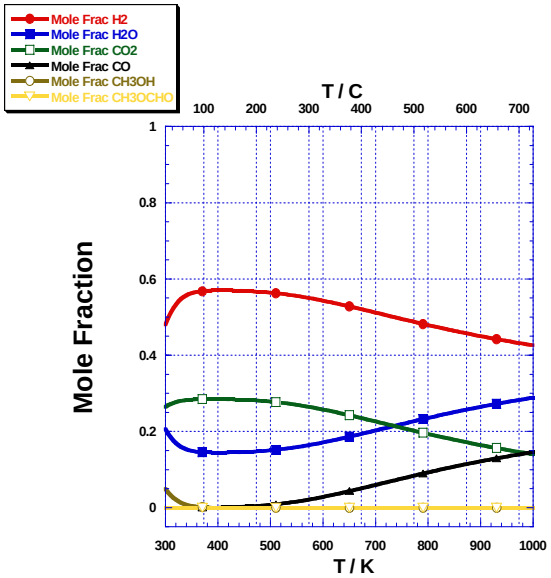

Figure 3. 12 Mole fraction of products from steam reforming of methyl formate at 1 bar and S/C = 1.5

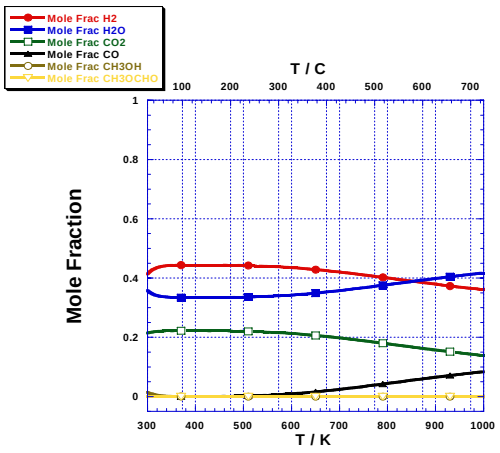

Figure 3. 14 Mole fraction of products from steam reforming of methyl formate at 1 bar and S/C = 2.5

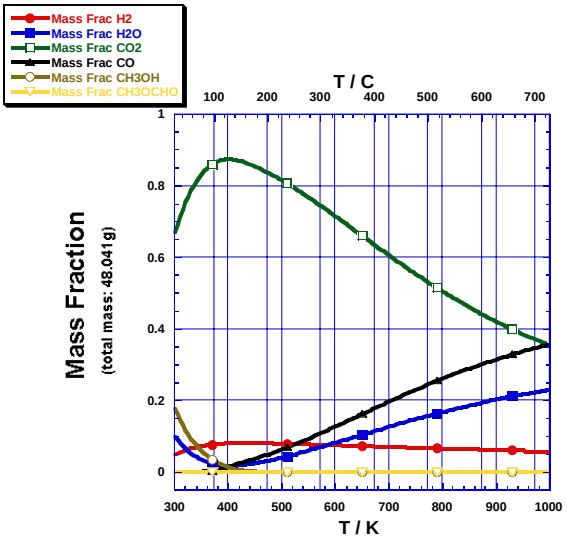

Figure 3. 15 Mass fraction of methyl formate products at 1 bar and S/C = 1. As with methanol, CO_2 dominates the mass fraction plots at approximately 80% for S/C = 1 and 1.5 and approximately 60% for S/C = 2 and 2.5

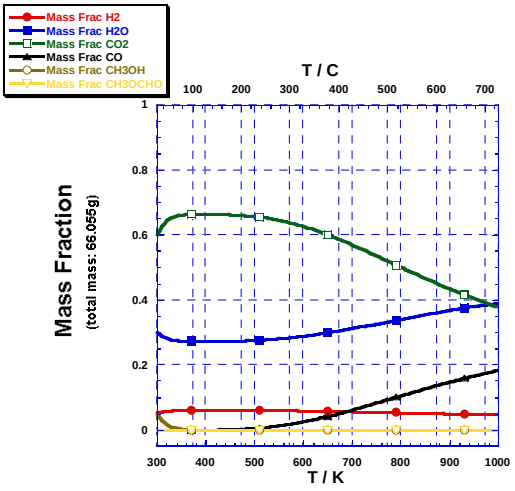

Figure 3. 17 Mass fraction of products from steam reforming of methyl formate at 1 bar and S/C = 2

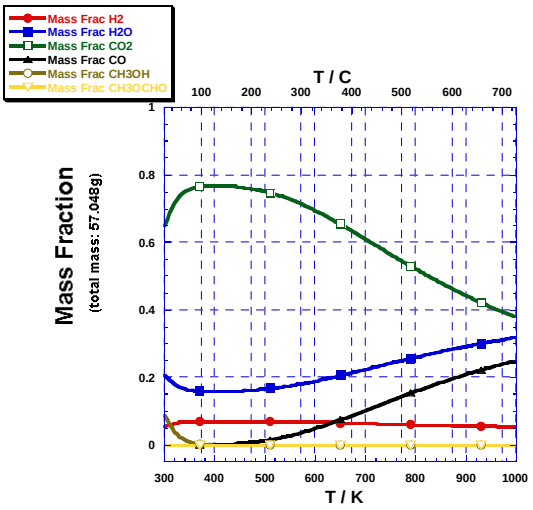

Figure 3. 16 Mass fraction of methyl formate products at 1 bar and S/C = 1.5

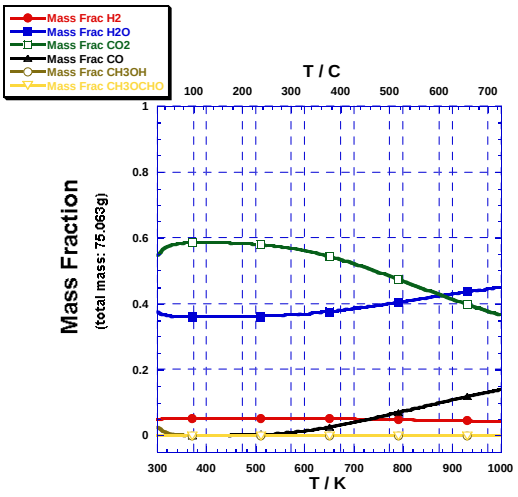

Figure 3. 18 Mass fraction of products from steam reforming of methyl formate at 1 bar and S/C = 2.5

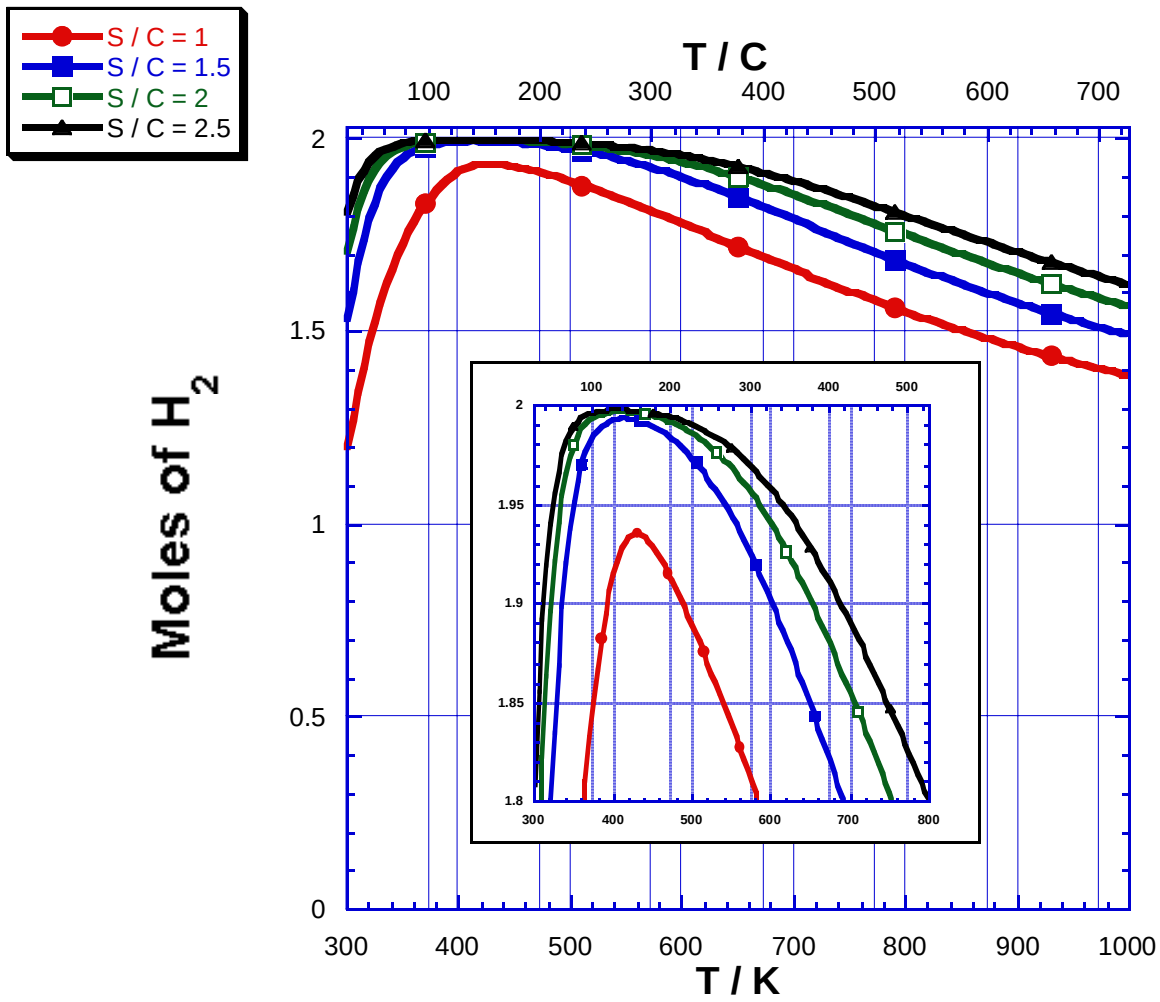

Figure 3. 19 H_2 production from steam reforming of methyl formate at 1 bar varying steam to carbon ratio. The H_2 curves show the characteristic rise and shift to lower temperatures the peaks. Resembling methanol, these curves also display a substantial broadening of their maximum values and lengthening of the range of operating temperatures

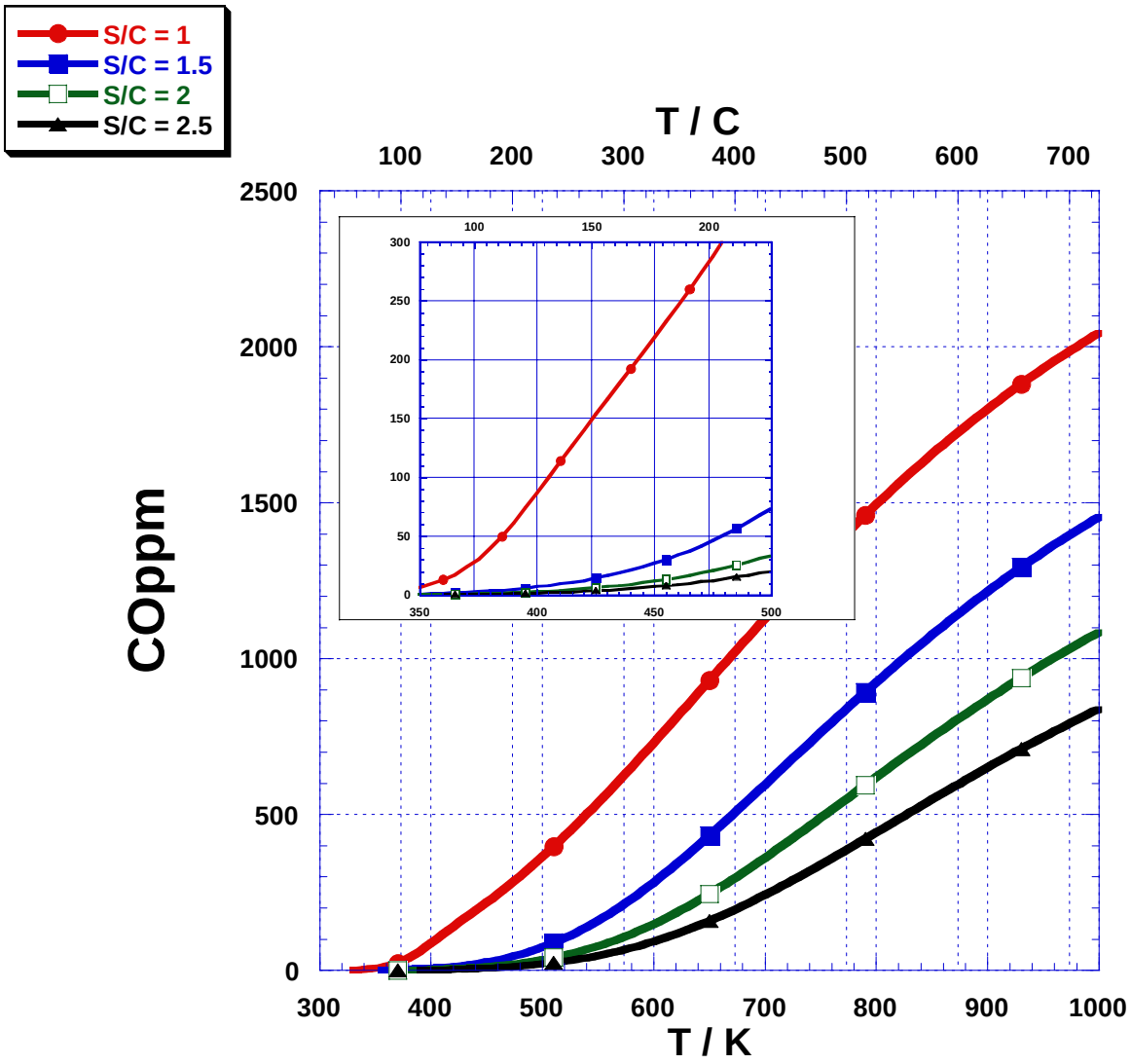

Figure 3. 20 CO production from steam reforming of methyl formate at 1 bar varying steam to carbon ratio. Table 3.2 provide supplementary details.

3.4 Dimethyl Ether

Figures 3.21-3.24 are the mole fraction plots for products from steam reforming of dimethyl ether (DME). DME displays a slightly more complex response to increasing the S/C ratio of the feed. The chemical formula of steam reforming of DME is listed again as equation 3.5. Table 3.3 demonstrates how the coefficients of the products change with X, the S/C ratio.

$$\tfrac{1}{2}CH_3OCH_3 + x\ H_2O \Leftrightarrow \psi\ H_2O + \alpha\ CO + \beta\ CO_2 + \gamma\ H_2 \qquad (3.5)$$

Table 3. 3 Steam reforming of DME product coefficients as a function of S/C ratio

	ψ	α	β	γ
S/C = 1	0	0.5	0.5	2.5
S/C = 1.5	0	0	1	~3
S/C = 2	0.5	0	1	3
S/C = 2.5	1	0	1	3

The DME's mole fraction figures show that the fraction of H_2 increases from 71 to 73% as the S/C ratio rises from 1 to 1.5. This rise it mole fraction with increasing steam is quite a departure from the responses of either methanol or methyl formate because the molar quantity of H_2 actually increases as table 3.3 demonstrates.

Figures 3.25-3.28 show the mass fraction of products from the steam reforming of DME. Again, CO_2 is the majority mass produced. However, the fraction of CO_2 is greater for S/C =1.5 than for S/C = 1. The increased mass of steam oxidizes CO to create CO_2. Increasing the S/C ratio beyond 1.5 decreases the CO_2 mass fraction as CO_2 is saturated. Figure 3.29 shows the H_2 moles produced from the steam reforming of DME. When compared to methanol and methyl formate, DME's H_2 curves display an exaggerated rise and shift with increasing feed steam. The peak of H_2 production rises from 2.5 to 3 moles and shifts from 500 to 414K. Warming 1mole of water to 500K from room temperature costs 70.9KJ. Only an additional 7.5KJ is needed to warm 2.5 moles

of water at room temperature to steam at 415K. Figure 3.30 and table 3.4 give details of CO produced from reforming of DME. The ratio of carbon to oxygen in DME reforming is 1:2 as with methanol and methyl formate. However, reforming DME produces comparatively more CO than the other fuels. Even with S/C = 2, DME produces more CO than either methanol or methyl formate produce with S/C = 1.5. More steam is needed to drive DME reforming to completion.

Table 3. 4 CO content of DME reformate gas at temperature of maximum H_2 production

	CO (ppm)	T (K)
S/C = 1	1450	500
S/C = 1.5	200	455
S/C = 2	16	424
S/C = 2.5	5.5	415

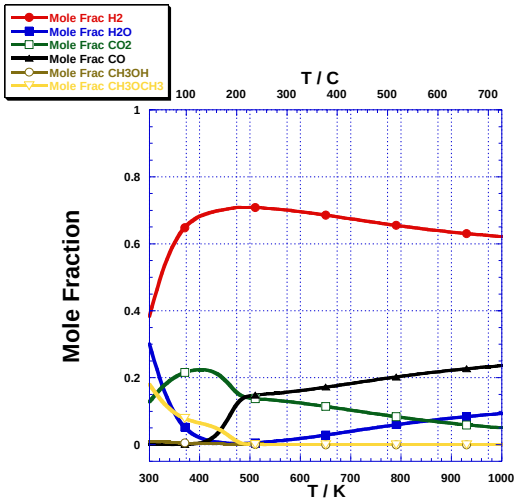

Figure 3. 21 Mole fraction of dimethyl ether products at 1 bar and S/C = 1. The DME's mole fraction figures show that the fraction of H_2 increases from 71 to 73% as the S/C ratio rises from 1 to 1.5

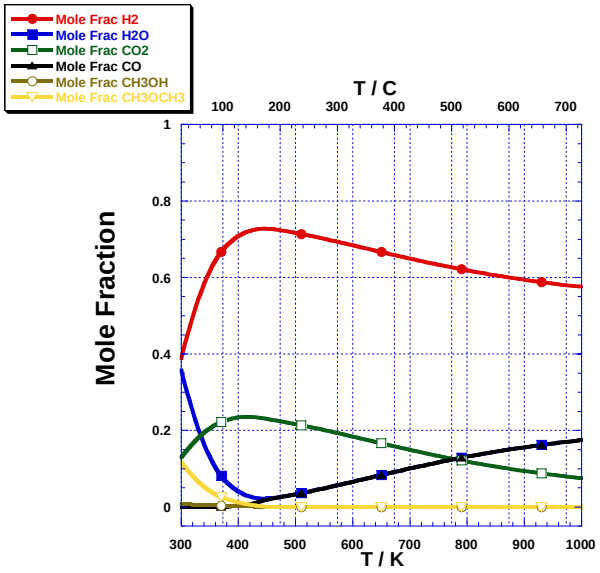

Figure 3. 22 Mole fraction of dimethyl ether products at 1 bar and S/C = 1.5. This rise it mole fraction with increasing steam is quite a departure from the responses of either methanol or methyl formate because the molar quantity of H_2 actually increases

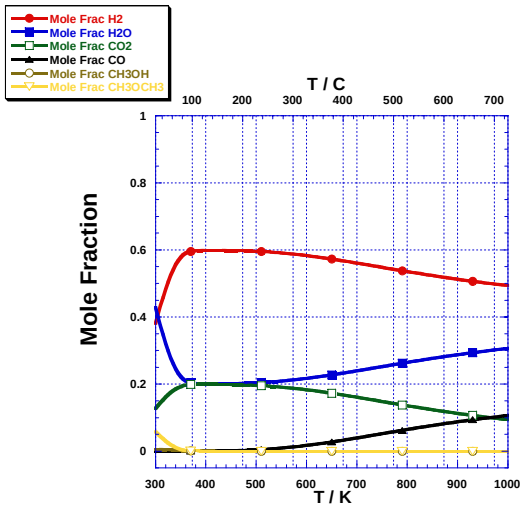

Figure 3. 24 Mole fraction of products from steam reforming of dimethyl ether at 1 bar and S/C = 2.5

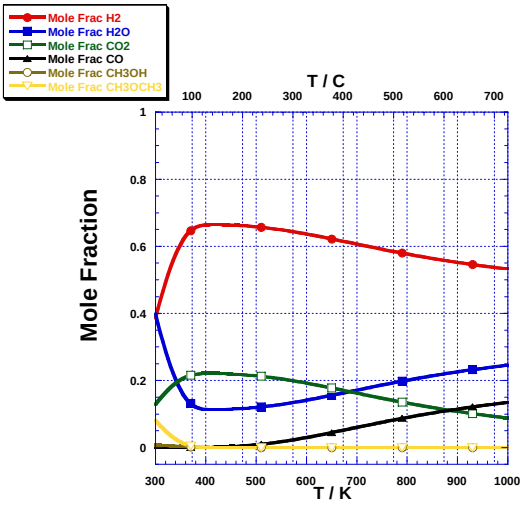

Figure 3. 23 Mole fraction of products from steam reforming of dimethyl ether at 1 bar and S/C = 2

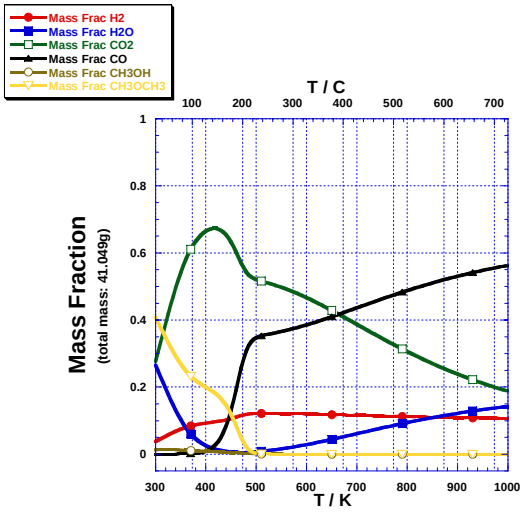

Figure 3. 25 Mass fraction of dimethyl ether products at 1 bar and S/C = 1. The fraction of CO_2 is greater for S/C =1.5 than for S/C = 1. The increased mass of steam oxidizes CO to create CO_2.

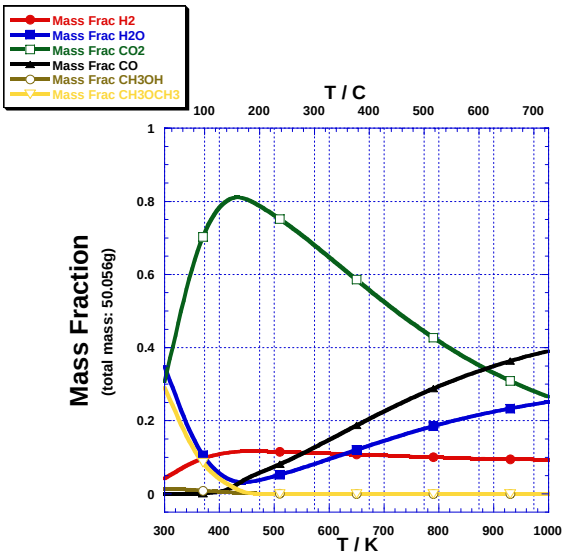

Figure 3. 26 Mass fraction of dimethyl ether products at 1 bar and S/C = 1.5

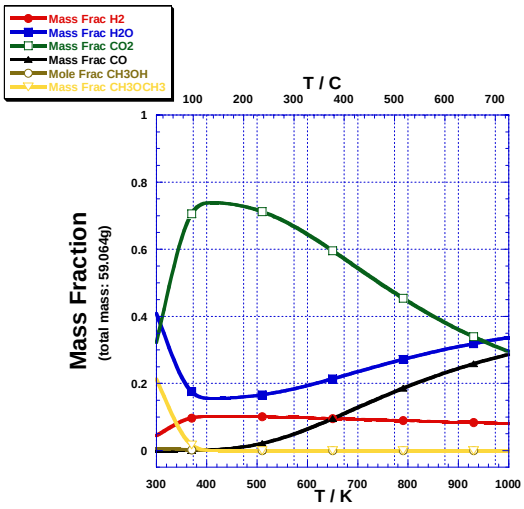

Figure 3. 27 Mass fraction of products from steam reforming of dimethyl ether at 1bar and S/C =2

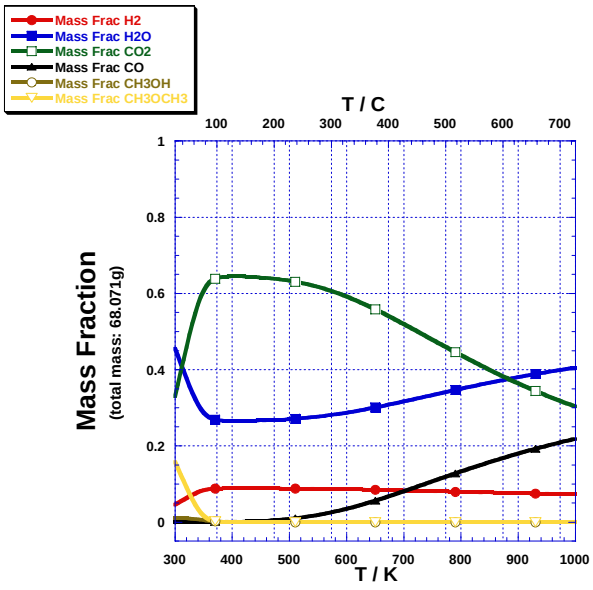

Figure 3. 28 Mass fraction of products from steam reforming of dimethyl ether at 1 bar and S/C = 2.5

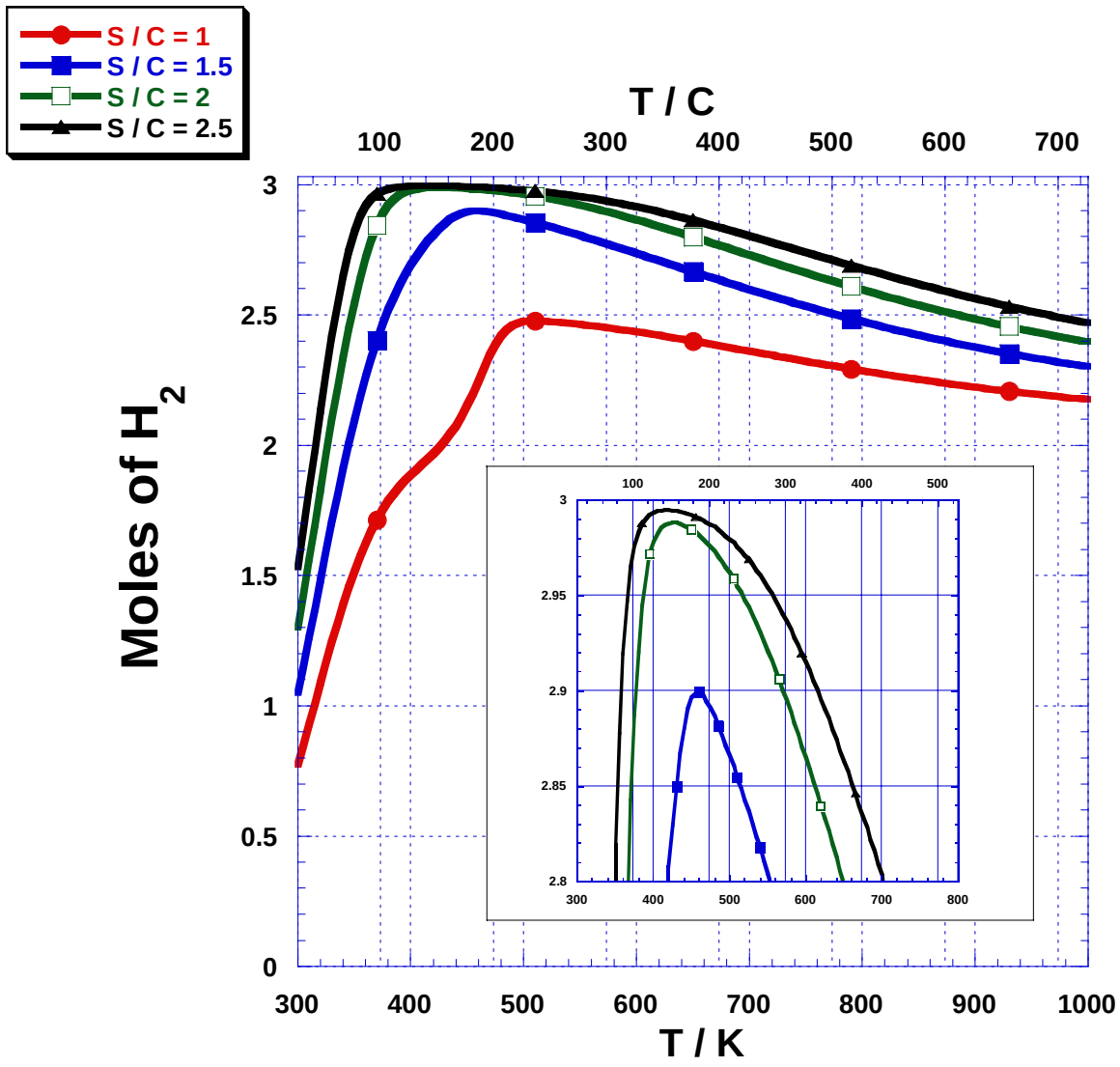

Figure 3. 29 H_2 production from steam reforming of dimethyl ether at 1 bar varying steam to carbon ratio. When compared to methanol and methyl formate, DME's H_2 curves display an exaggerated rise and shift with increasing feed steam

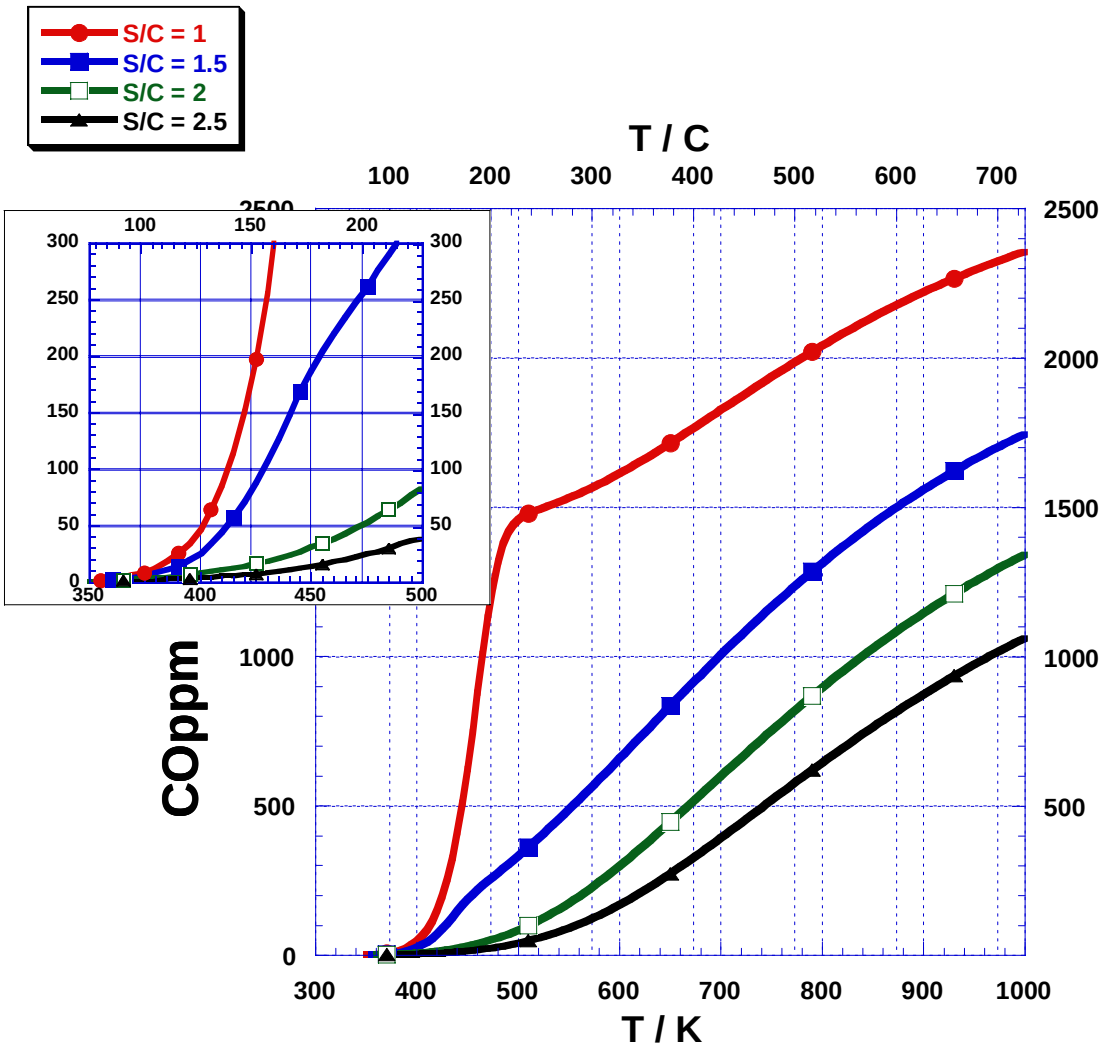

Figure 3. 30 CO production from steam reforming of dimethyl ether at 1 bar varying steam to carbon ratio. More steam is needed to drive DME reforming to completion.

3.5 Conclusion

A Comparison of the characteristics of each reforming fuel will determine how to best use the fuels to maximize H_2 yield and minimize the CO content. Thermodynamics show that if methanol is reformed at a temperature of 416K and S/C = 1.5, 2.99 moles of H_2 can be generated, a yield of 96.7%, with 13ppm of CO. If methyl formate is reformed at 411K and S/C = 1.5, it can produce 1.99 moles of H_2, a 96.5% yield, and 9.8ppm of CO. DME, if reformed at 424K and S/C = 2, will produce 2.99 moles of H_2, a 96.7% yield, and 16ppm of CO.

CHAPTER 4

QUASI EQUILIBRIUM ANALYSIS OF H_2 GENERATION BY PYROLYSIS OF SMALL HYDROCARBONS

4.1 Introduction

Another effective means to generate hydrogen is from the pyrolysis of hydrocarbons. In the present chapter, the thermodynamic boundaries of the pyrolysis of methane and ethane are explored. Pyrolysis is a chemical reaction brought about by the action of heating. In practice, it is also necessary to cool rapidly to avoid accumulation of solid carbon deposits. Hydrocarbon pyrolysis is an endothermic reaction for which the molecules enthalpy of formation, ΔH_f, provides a measure of how much heat is needed to crack the reactant fuels and to form the products. Figure 4.3 is a plot of ΔH_f for several hydrocarbon molecules and is relatively constant across a large temperature range. ΔH_f is the energy required to form a compound from its elements in their reference state, or their most stable state, for a specified temperature at 1 bar [28]. The difference in ΔH_f for two compounds gives a measure of how much energy is required to form one compound from the other. If the starting fuel is methane, CH_4, with an average ΔH_f of -85KJ, it will take 195KJ to form acetylene, C_2H_2, which has an average ΔH_f of 110KJ. The area between methane and acetylene compared to other hydrocarbons show that the synthesis route between the two is the most energy intensive. Thus, it can be expected that the formation of acetylene from methane will take the highest temperatures. Since the difference

between the ΔH_f curves of ethane and other hydrocarbons is less than the difference between these and methane, as illustrated in figure 4.3, one can anticipate that ethane pyrolysis will require less energy, and thus takes place at lower temperatures, than methane pyrolysis.

The ΔH_f curve of methane has the lowest value because of its relative high stability compared to the other compounds in figure 4.1. Since ΔH_f for carbon and hydrogen is zero at all temperatures, methane also has high stability when compared to its elements. Given that ΔH_f is the energy need to form a compound from its elements, the negative value of ΔH_f for methane suggests that carbon and hydrogen can release energy and obtain a lower state when they combine to form methane, similarly for ethane. The structure of methane is a single carbon bonded to four hydrogen atoms as in figure 4.1 and ethane is similar to ethane except that it contains one carbon-carbon (C-C) bond as in figure 4.2.

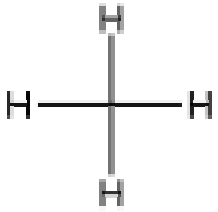

Figure 4. 1 CH_4

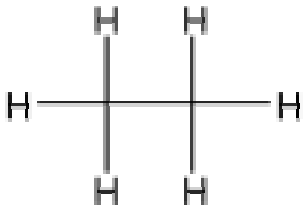

Figure 4. 2 C_2H_6

The bond dissociation enthalpy, $\Delta H(A\text{-}B)$, is the reaction enthalpy for the breaking of the bond A-B. The standard dissociation enthalpy of a carbon-hydrogen bond, $\Delta H(C\text{-}H)$, equals 412KJ mol^{-1} and a single carbon bond $\Delta H(C\text{-}C)$ is 348KJ mol^{-1}. A comparison of

the dissociation enthalpies shows that breaking a C-C bond costs 12% less energy than breaking a C-H bond. The relative stability of methane with respect to other hydrocarbons is a consequence of the difference in dissociation enthalpies. Since methane is the simplest of hydrocarbons and since methane contains no C-C bonds it is comparatively uncreative. Due to its simplistic structure, methane can not be fractionated into lighter hydrocarbons, but instead, it undergoes coupling to form higher hydrocarbons [29]. Ethane, used as a fuel, has the ability to undergo both fractionation and coupling to create other hydrocarbons.

The enthalpy of formation is not the only necessary indication of the energy or reaction temperature that will be needed to enable a pyrolysis reaction to occur. While ΔH_f tells how much energy is needed to form one compound from another, the Gibbs free energy of formation, ΔG_f, gives the relative stability of molecules. In order for a chemical process to go forth at a specified temperature, the products must be stable with respect to the reactants and the temperature must be such that the required energy is imparted to the reaction. Figure 4.4 is a plot of the ΔG_f versus temperature of the same compounds found in figure 4.3. If methane is used as a starting material, figure 4.4 is determinative of which products can be generated and in which order. The lower the ΔG_f, the more stable is a compound. The point at which the methane curve is above the curve of another compound, is the pointy at which methane is less stable and the formation that compound is thermodynamically favorable. From figure 4.4, pyrolysis of methane would first allow for the decomposition of methane into its elements at roughly 875K since ΔG_f of H_2 and C are both equal to zero (not shown in figure 4.4) and since the methane ΔG_f

curve crosses the zero line at 875K. Kinetic constraints prevent the process of methane or ethane decomposition; accordingly, decomposition will not be an included process in the present thermodynamic model. Secondly, the methane curve crosses naphthalene, $C_{10}H_8$, and benzene, C_6H_6, at 1300K. At 1500K and 1600K acetylene, C_2H_2, and ethylene, C_2H_4, become respectively more stable than methane. Due to the negative slope of the C_2H_2 curve acetylene will become the most stable of all of the compounds and will be the dominant pyrolysis product at higher temperatures. Ethane's ΔG_f curve intersects all of the other hydrocarbons at lower temperatures than did methane. Therefore, if ethane is the starting material, pyrolysis can occur at lower temperatures than for methane. Ethane's ΔG_f curve crosses naphthalene and benzene at 825K. Differing from methane, ethane crosses the C_2H_4 curve before it crosses the C_2H_2 curve, 1173K and 1225K respectively. In addition to meeting the other hydrocarbon curves, the ethane pyrolysis favors the production of methane since the ethane curve is always above methane's.

4.2 Pyrolysis Calculations

Gibbs free energy minimization is employed to analyze the pyrolysis of ethane and methane. In the present investigation, seven compounds are considered to be involved in catalyzed pyrolysis of ethane and methane. The compounds are ethane, methane, acetylene, ethylene, benzene, naphthalene, and molecular hydrogen. Although it is not necessary for the calculation, a listing of the possible pyrolysis reactions is helpful for conceptualization. The above mentioned compounds react to generate H_2 from ethane and methane in the following ways.

4.21 Ethane Equations

$$C_2H_6 \Leftrightarrow \alpha\ C_2H_2 + \beta\ H_2 \quad (4.1)$$

$$C_2H_6 \Leftrightarrow \chi\ C_2H_4 + \delta\ H_2 \quad (4.2)$$

$$C_2H_6 \Leftrightarrow \varepsilon\ C_6H_6 + \gamma\ H_2 \quad (4.3)$$

$$C_2H_6 \Leftrightarrow \kappa\ C_{10}H_8 + \lambda\ H_2 \quad (4.4)$$

$$C_2H_6 \Leftrightarrow \sigma\ CH_4 + \varpi\ C_{10}H_8 + \xi\ H_2 \quad (4.5)$$

4.22 Methane Equations

$$CH_4 \Leftrightarrow A\ C_2H_2 + B\ H_2 \quad (4.6)$$

$$CH_4 \Leftrightarrow X\ C_2H_4 + \Delta\ H_2 \quad (4.7)$$

$$CH_4 \Leftrightarrow E\ C_6H_6 + \Gamma\ H_2 \quad (4.8)$$

$$CH_4 \Leftrightarrow K\ C_{10}H_8 + \Lambda\ H_2 \quad (4.9)$$

Since the stability of product formation is heavily temperature dependent, the coefficients of each compound, Greek letters, in equation 4.1 – 4.9 are dependant on the temperature at which pyrolysis reactions are carried out. At a specified temperature, pyrolysis of ethane will produce a yield given by a combination of equations 4.1 – 4.5. In the same way, pyrolysis of methane yields a combination of equations 4.6 – 4.9.

4.3 Results of Calculations

Figures 4.5 and 4.6 are results from ethane pyrolysis calculations at 1 bar and from 500 – 1800K. The mole fraction plot can be compared to equations 4.1 – 4.5 to provide a sense of the selectivity of products and the magnitude of coefficients in the equations. Again, from figure 4.4, methane is the most stable hydrocarbon at low to moderate temperatures; hence methane is expected to be an immediate product of ethane pyrolysis at temperatures lower than 825K when the ethane ΔG_f curve intersects the curves of benzene and naphthalene. Figure 4.5 illustrates that at low temperatures CH_4 and $C_{10}H_8$ are the primary products; thus equation 4.5 is the route for ethane pyrolytic conversion. At high temperatures, figure 4.5 shows the primary products are H_2 and C_2H_2 making equation 4.1 ethane's pyrolytic path. Intermediate temperatures show ethane pyrolysis to shift gradually from exclusively equation 4.5 to exclusively equation 4.1. The mass fraction plot, figure 4.6, is another way to observe the order of product formation. At low temperatures ethane pyrolysis, to a large degree, produces only methane. At 500K, 30g of ethane (1 mole) generates 22g of CH_4 and 7.8g of C_8H_{10}. CH_4 and C_8H_{10} generation are fairly constant with decreasing temperature until a decline in CH_4 is noticed just above 825K. The decline in methane generation is coincident with a rise in creation of C_6H_6, $C_{10}H_8$ and H_2. C_6H_6 and $C_{10}H_8$ have simultaneous peaks just below 1500K at 6.3g and 13.5g respectively. Just above 1500K, production of C_6H_6 and $C_{10}H_8$ experience a decline which is coincident with a rise in production of C_2H_2. Production of C_2H_2 peaks at 1800K with a mass of 24.6g and a H_2 mass of 3.9g. The masses of C_2H_2 and H_2 at 1800K account for 95% of the initial mass of ethane.

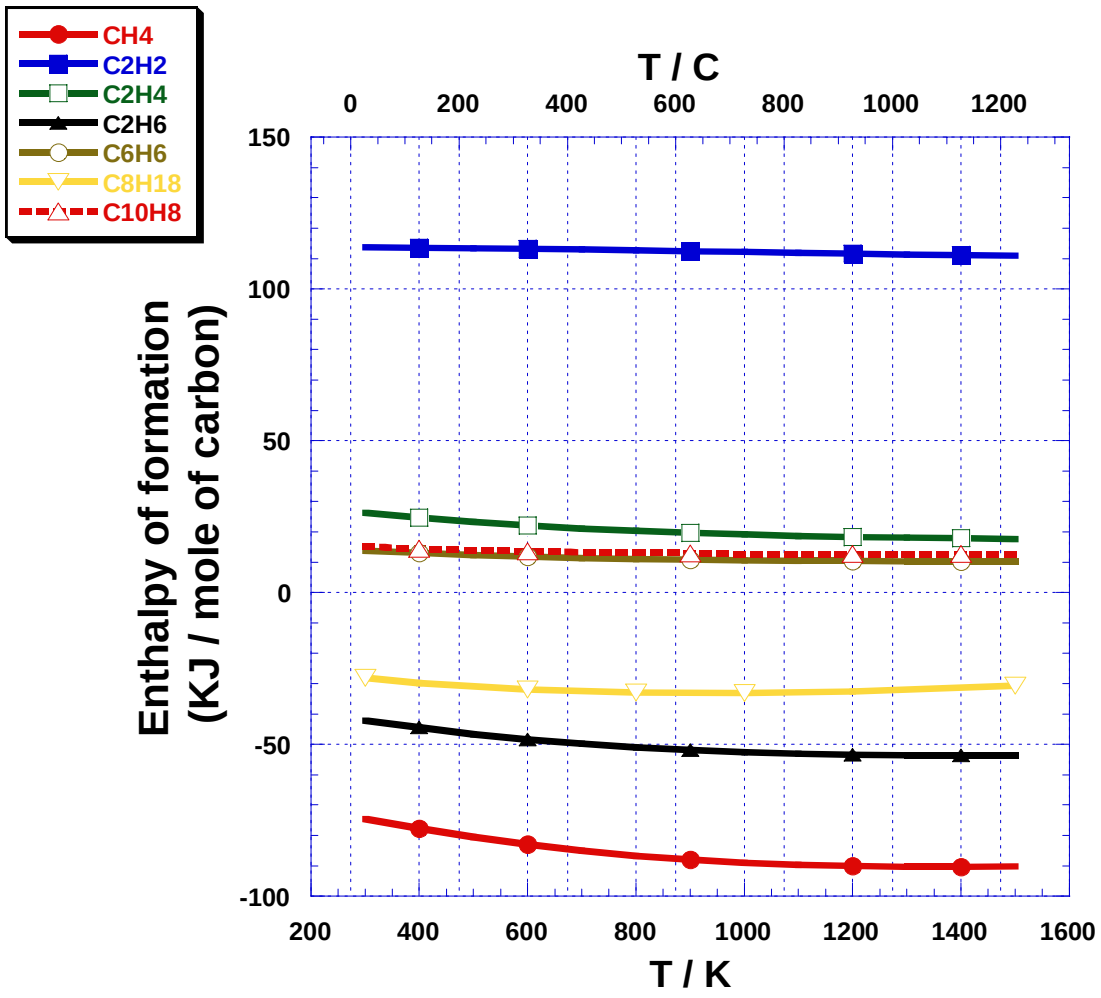

Figure 4. 3 Comparison of formation enthalpy (ΔH_f) of different hydrocarbons as a function of temperature. ΔH_f tells how much energy is needed to form one compound from another.

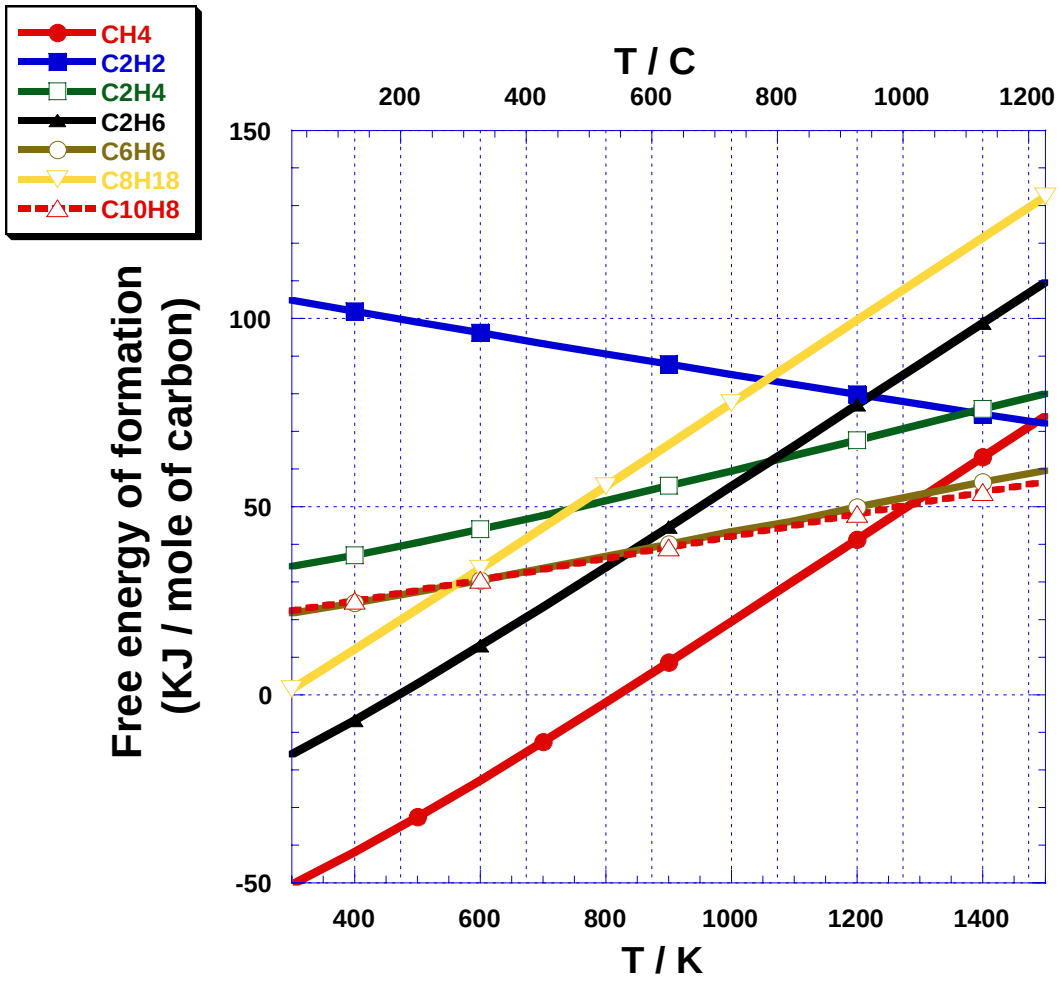

Figure 4. 4 Thermodynamic stability of several hydrocarbons at 1 bar and as a function of temperature. The lower the ΔG_f the more stable is a compound. At the point at which the methane or ethane curves are above the curve of another compound, methane or ethane is less stable and the formation that compound is thermodynamically favorable.

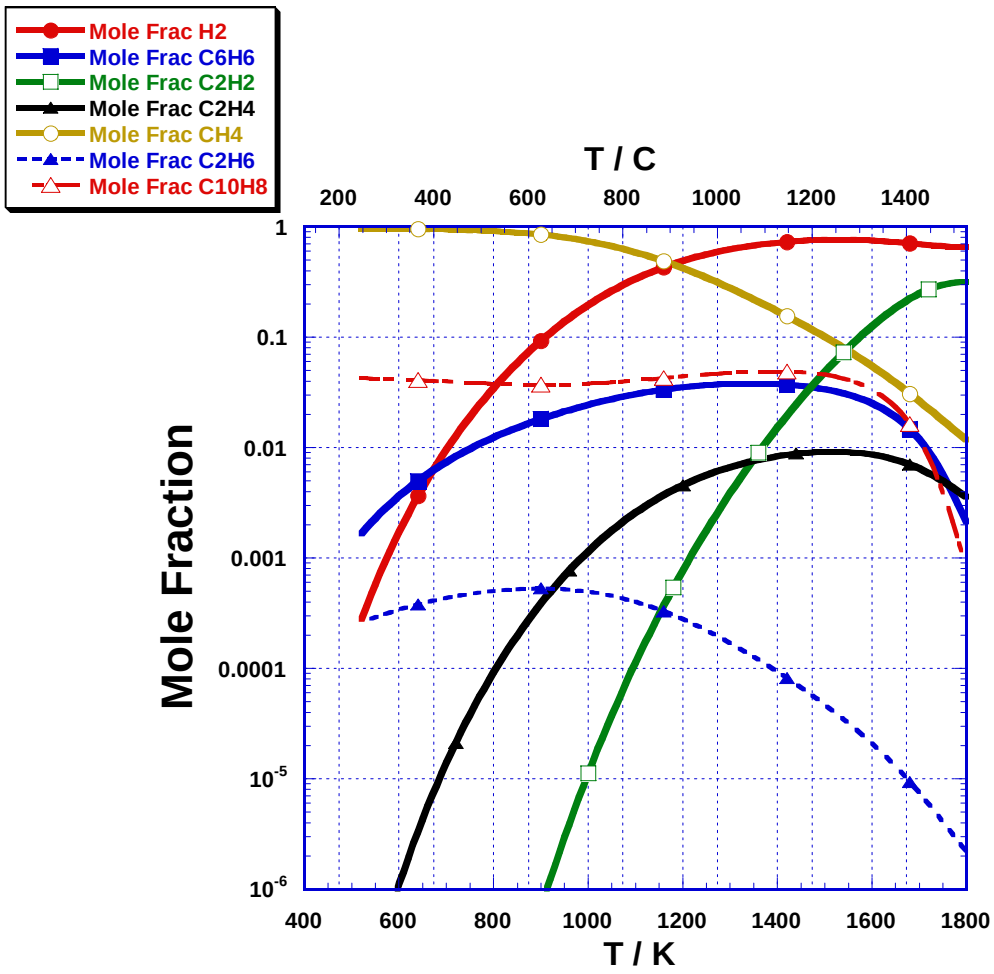

Figure 4. 5 Results from ethane pyrolysis calculations at 1 bar and from 500 – 1800K. The mole fraction plot can be compared to equations 4.1 – 4.5 to provide a sense of the selectivity of products and magnitude of coefficients in the equations.

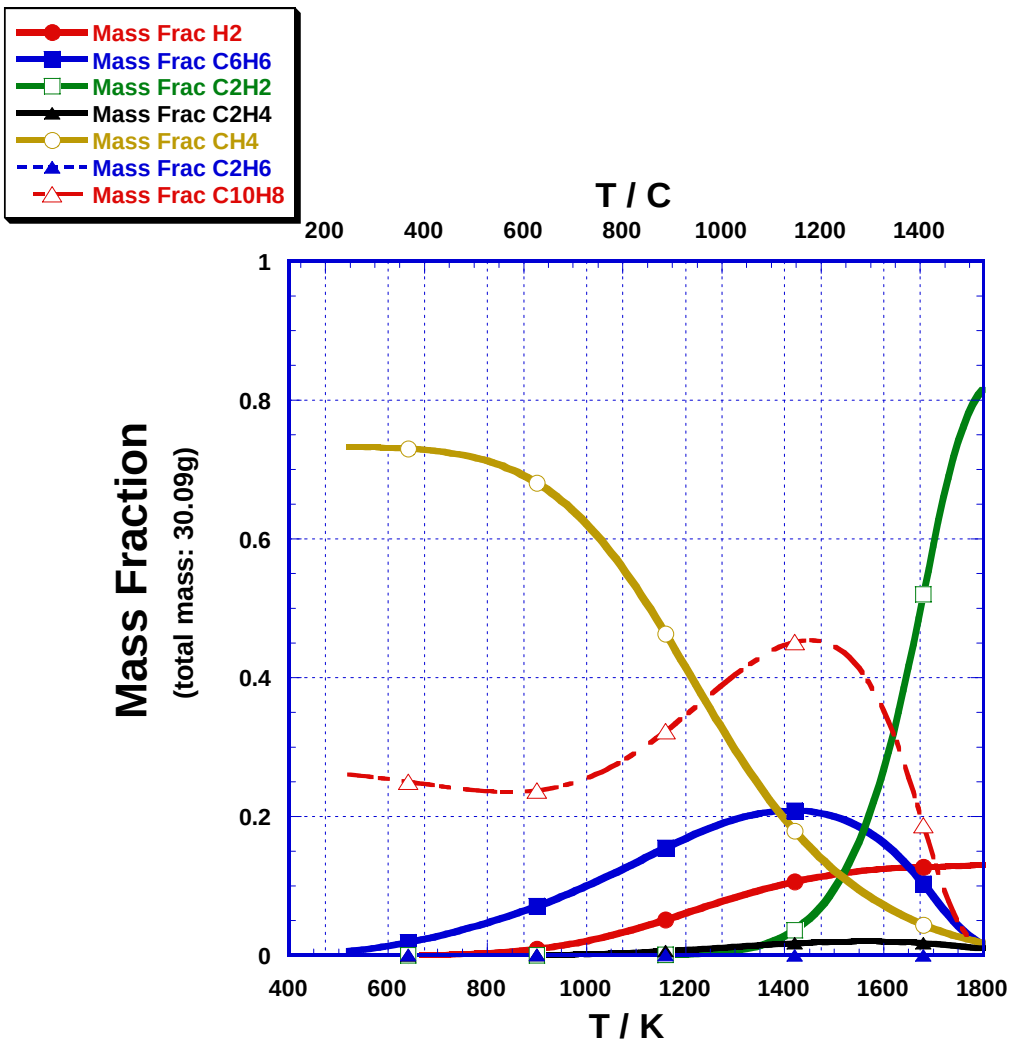

Figure 4. 6 The mass fraction of ethane pyrolysis. This plot provides a way to observe the order of product formation versus temperature.

Figures 4.7 and 4.8 are results from methane pyrolysis calculations at 1 bar and from 500 – 1800K. Figure 4.7 shows methane to be resilient to pyrolytic transition to higher hydrocarbons until just below 1200K. The mole fraction plot illustrates a steady increase of C_6H_6, $C_{10}H_8$ and H_2 even at the lowest temperatures. The model predicts that C_6H_6 and $C_{10}H_8$ could be detected at 1-10 parts per million (ppm) between 600 and 800K,

10-100 ppm between 800 and 1000K, and 100-200 ppm between 1000 and 1500K. After 1500K there is a noticeable drop in the mole fraction of C_6H_6 and $C_{10}H_8$. C_2H_4 is also produced at low temperatures and can be detected at one tenth of the level of C_6H_6 and $C_{10}H_8$ for much of the plot. Though figure 4.4 demonstrates the relative stabilities of hydrocarbons and thus the conversion temperatures from methane, figure 4.7 shows that products can form from methane even at low temperatures but at scarcely detectable levels.

H_2 is produced over the entire temperature range of figure 4.7 together with the production of all of the hydrocarbons according to equations 4.6 – 4.9. H_2 is produced from methane first by equation 4.9, then by 4.8, 4.7 and then finally by 4.6. Comparing methane and ethane by their H_2 production, figures 4.9 and 4.10, make clear that at 1500K, one mole of ethane produces 1.8 moles of H_2 and one mole of methane produces 1.4 moles of H_2. Nevertheless, methane's mass fraction of H_2 at 1500K is 16% to ethane's 12.6%. Ethane can produce more H_2, but methane produces H_2 more efficiently. The curves for H_2 in figures 4.9 and 4.10 rise sharply above 800K and level off above 1500K. If the goal for the pyrolysis reaction is ultimately to produce H_2, temperatures above 1500K should be avoided since only a marginal increase in H_2 is realized from a large increase in temperature.

Figure 4.8 is a plot of mass fraction of products from methane pyrolysis. The model predicts that at 1200K 50% of methane is converted to benzene, naphthalene and hydrogen. Above 1200K and particularly above 1500K, pyrolysis of methane is through the conversion to acetylene which is in accordance with the decrease of C_2H_2's ΔG_f curve and the increase of all other curves in figure 4.4.

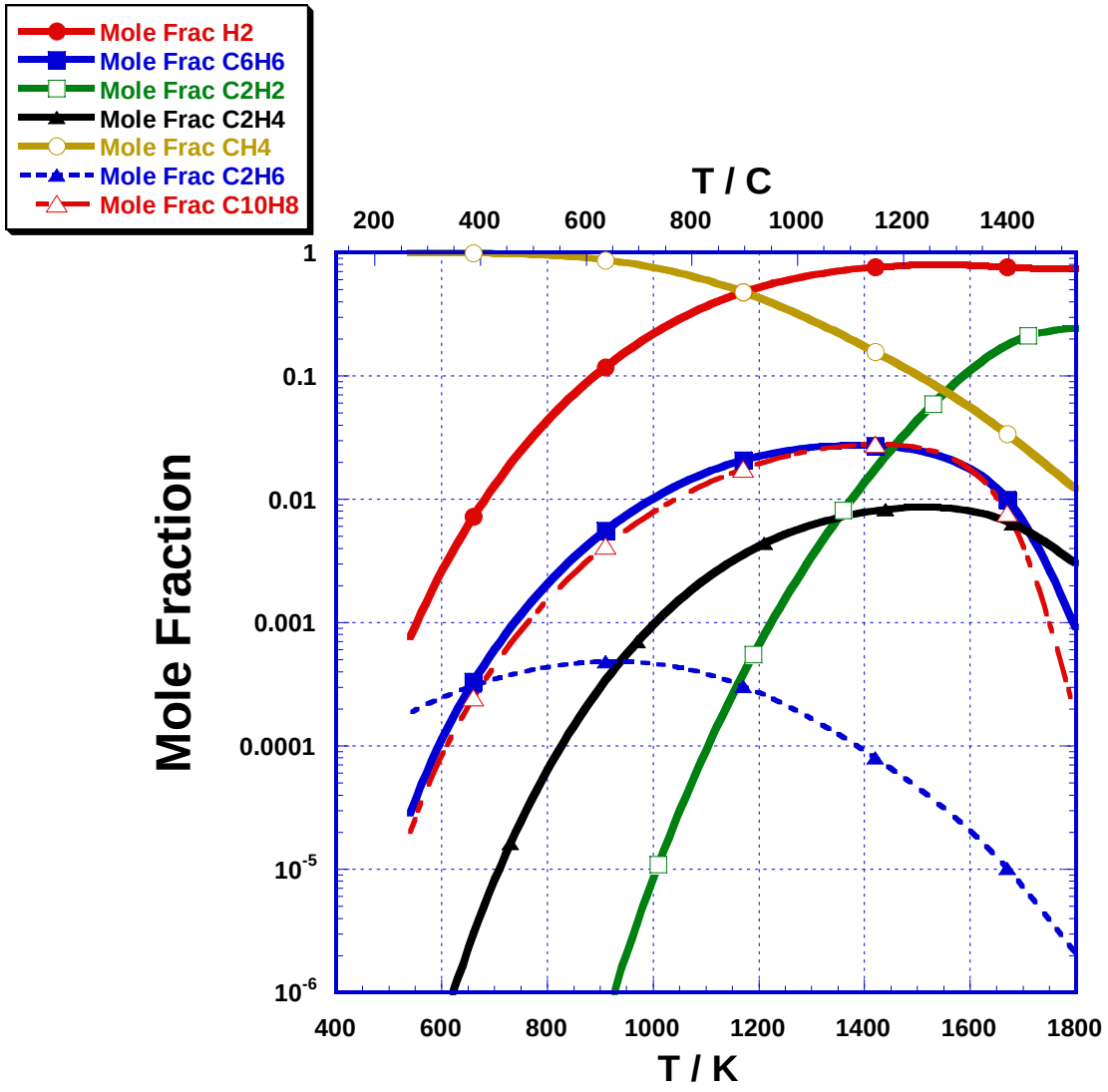

Figure 4. 7 Mole fraction of methane pyrolysis products. Methane is resilient to pyrolytic transition to higher hydrocarbons until just below 1200K

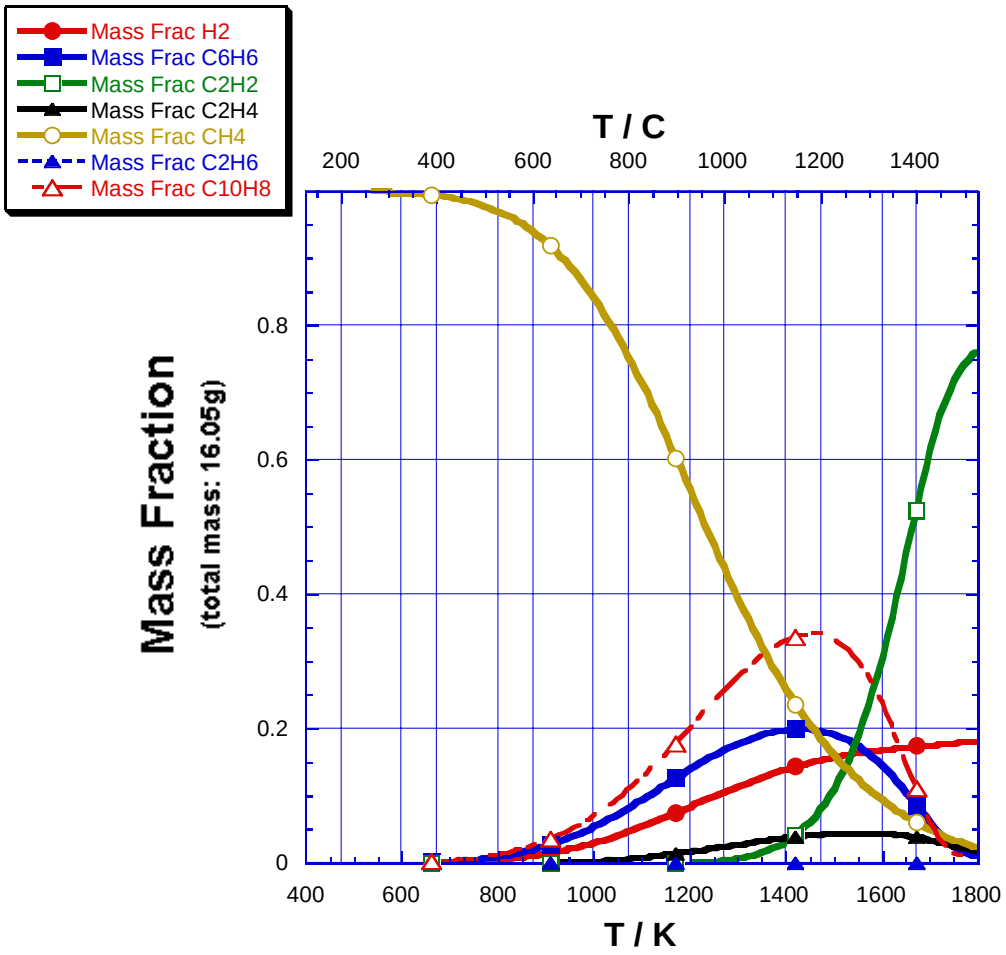

Figure 4. 8 Plot of mass fraction of products from methane pyrolysis. At 1200K 50% of methane is converted to benzene, naphthalene and hydrogen. Above 1500K, pyrolysis of methane is through the conversion to acetylene

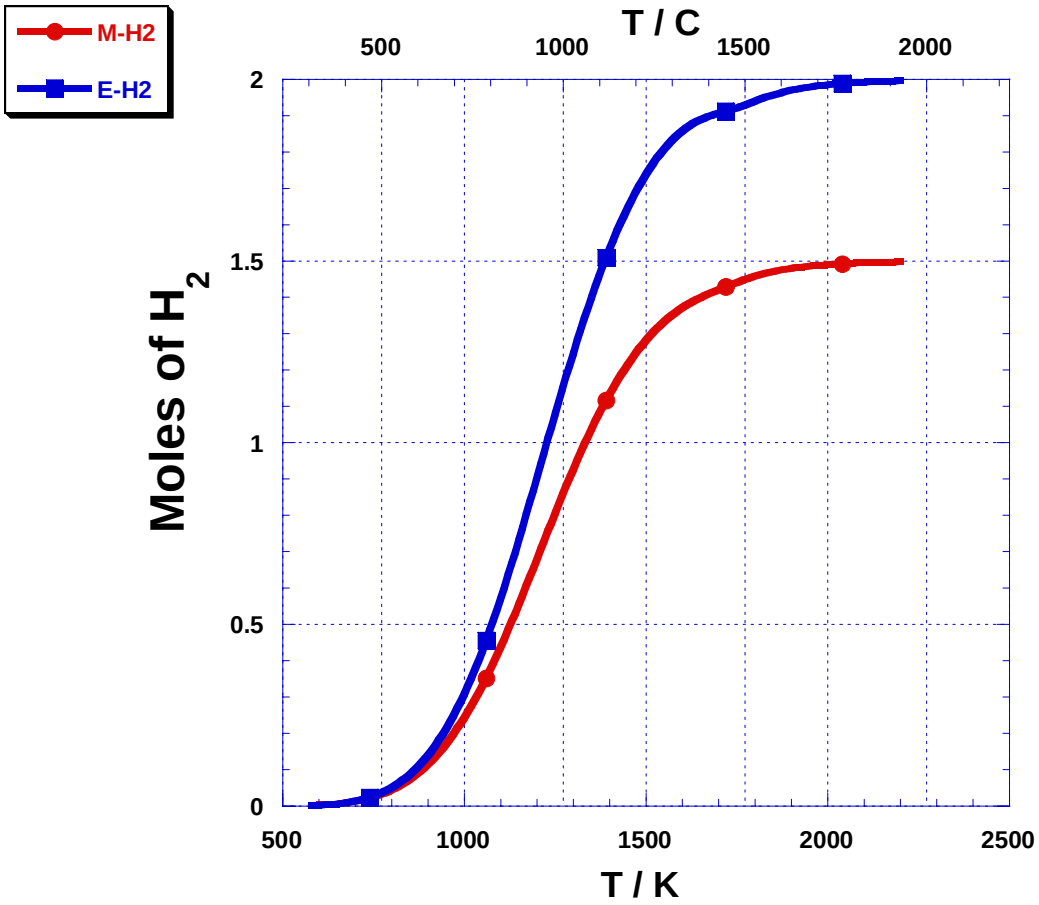

Figure 4. 9 Comparison of methane (red) and ethane (blue) by their H_2 production. At 1500K one mole of ethane produces 1.8 moles of H_2 and one mole of methane produces 1.4 moles of H_2.

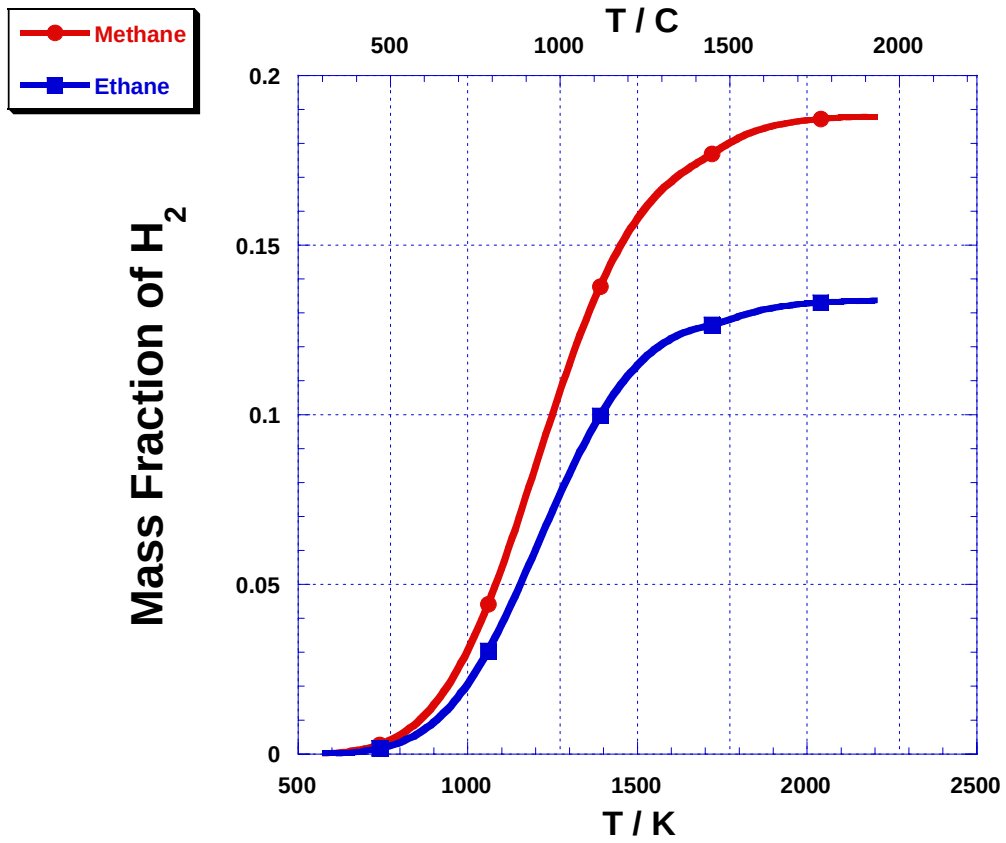

Figure 4. 10 At 1500K, methane's mass fraction of H_2 is 16% to ethane's 12.6%. Ethane can produce more H_2 but methane produces H_2 more efficiently

The dependence on pressure of the pyrolysis reaction is examined in figures 4.11 and 4.12 for ethane and methane respectively at 1475K. As pressure is decreased, productions of all hydrocarbons except for C_2H_2 are suppressed. In fact, the production of C_2H_2 is amplified with decreasing pressure. Therefore for each of the equations representing pyrolysis of ethane and methane, equations 4.1 and 4.6 are enhanced while all other equations are stifled. At 1 bar and 1475K, the coefficients of C_2H_2 and H_2 are 0.078 and 0.156 respectively for ethane and 0.05 and 0.15 respectively for methane. At

$5e^{-3}$ bar and 1475K, the coefficients of C_2H_2 and H_2 are 1 and 2 respectively for ethane and 0.5 and 1.5 respectively for methane. Equations 4.1 and 4.6 achieved their maximum stoichiometric values of C_2H_2 and H_2 from one mole of ethane or methane at 1475K. Data in figures 4.11 and 4.12 was taken at 1475K because it is near this temperature that generation of H_2 is at its peak. Further data taken at lower temperatures (not shown) reveals that production of C_2H_2 and H_2 can be brought up to their stoichiometric maximum values by decreasing pressure sufficiently. These pressure dependency results are agreement with other work [2].

4.4 Review of Experiments

Researchers[30],[31] have demonstrated that transporting ethane or methane through a catalytic heating region and allowing the gas to under go expansive cooling into a vacuum chamber, will generate other hydrocarbons and H_2. A scale drawing of the pyrolysis reactor is found in figure 4.14. In typical experiments, the reactant gas enters the reactor, or nozzle, at a pressure of about 20 torr at room temperature. Mass spectra of the emergent beam are recorded as the nozzle temperature is raised. The ambient pressure within the nozzle rises to about 85 torr at the highest temperature used, 1100° C. Typically, the flow rate through the reactor is of the order of 10^{19} molecules per second; the corresponding residence time for a molecule in the hot nozzle before emerging from the orifice is about 10 ms [4]. Conversion to higher hydrocarbons has been reported to reach nearly 100% for ethane and 70% for methane [3]. Figure 4.14 illustrates mass spectra from experiments showing product peaks of hydrocarbons, C_nH_m, where the most

abundant peaks are found for n = m. Peaks for even n are consistently stronger that neighboring odd n peaks especially in the range 3-6 [4].

A striking contrast between thermodynamic equilibrium and kinetic experiments is seen in ethane pyrolysis experiments. Thermodynamics shows prominent methane formation but the kinetic regime measures only scarce quantities [3]. The short contact time of pyrolysis selects the less energy consuming process of associating carbon atoms in C-C bonds considerably more so than that of C-H bonds. Thus higher hydrocarbon formation is augmented and methane formation is held to a mole fraction of 5%. Paradoxically, the same mechanism, strong C-H bonds, is likely responsible for both situations.

4.5 Conclusion

Quasi equilibrium calculations of pyrolysis show that ethane and methane can adequately produce H_2 at 1500K and at 1 bar. Ethane produces a 12% yield and methane produces a 16% yield per mole of fuel. Kinetic experiments show similar results but with less concentrations of CH_4 and $C_{10}H_8$.

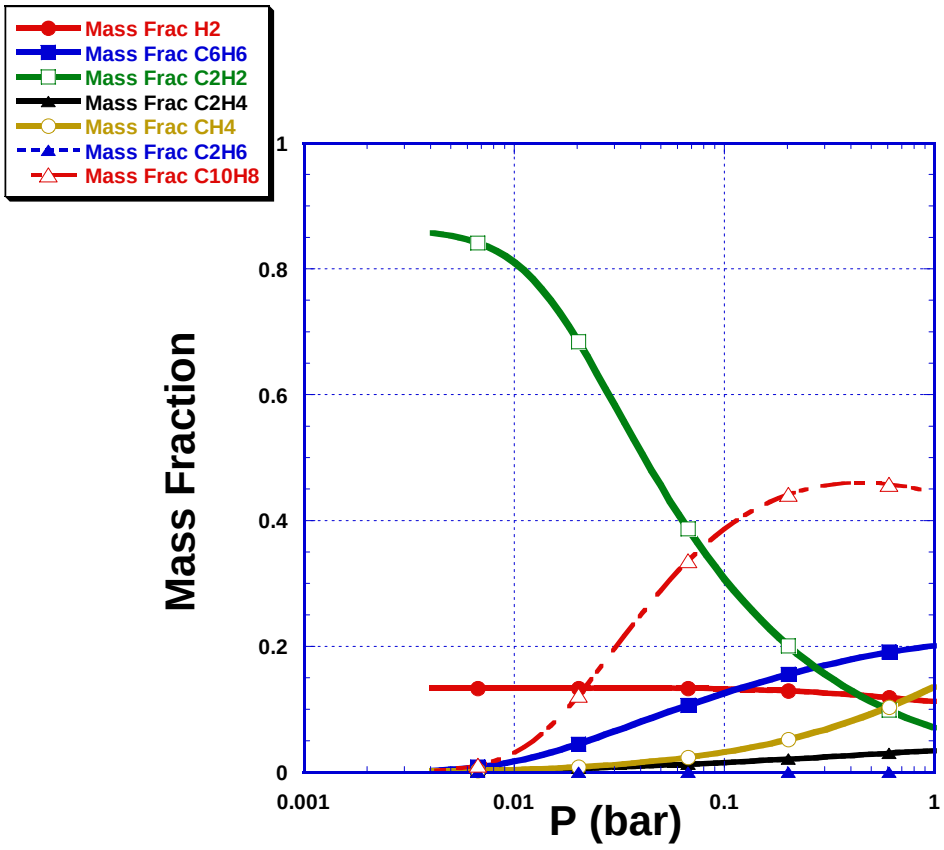

Figure 4. 11 Pressure dependence of pyrolysis reaction examined for ethane at 1475K. As pressure is decreased, production of all hydrocarbons except for C_2H_2 is suppressed.

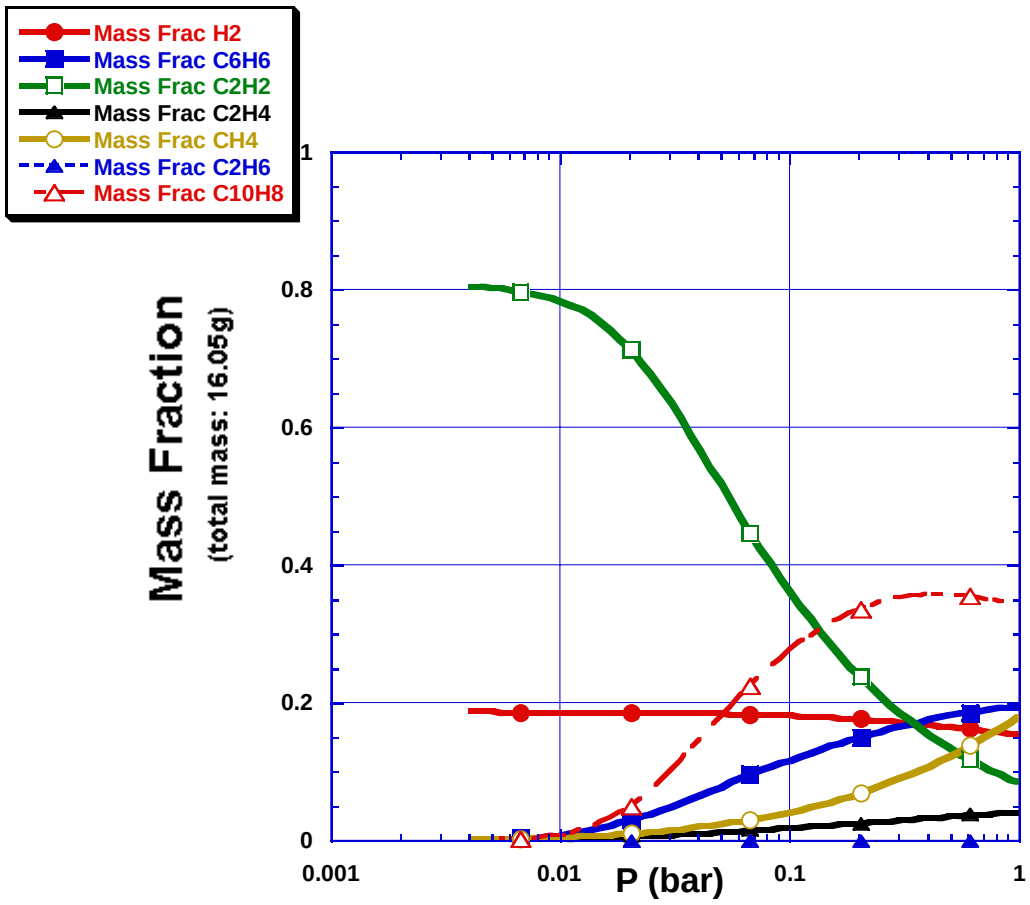

Figure 4. 12 Pressure dependence of methane pyrolysis reaction at 1475K. As with ethane pyrolysis, the production of C_2H_2 is amplified with decreasing pressure.

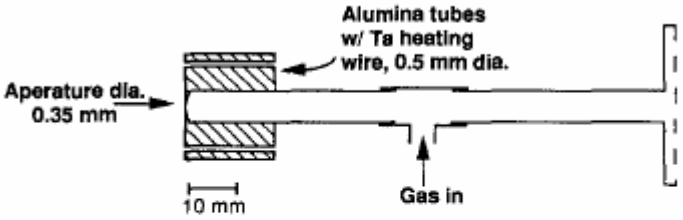

Fig. 1. Cut-away view of supersonic nozzle, drawn to scale. Nozzle body of nickel or molybdenum, with snout containing heaters and a tubular extension joined via a Swagelok coupling to a gas feed tube of thin-walled stainless steel. The Swagelok coupling permits easy detachment and a window (at right) aids alignment.

Figure 4. 13 Pyrolysis reactor. L. Shebaro et al.

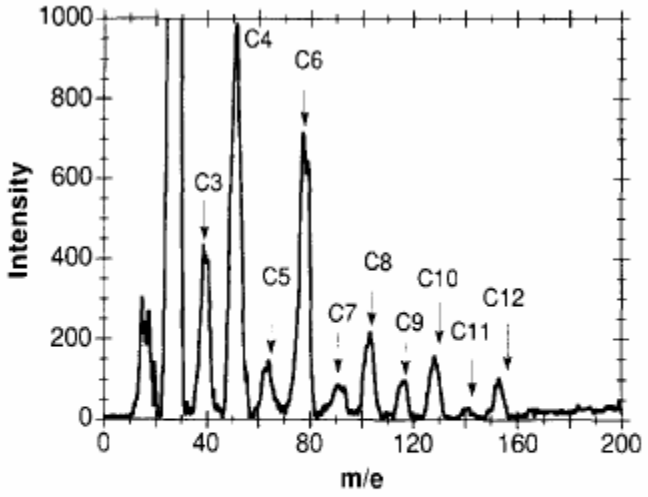

Fig. 2. Typical low resolution mass spectrum of products from ethane reactant (1060°C, 85 Torr) in Ni nozzle. Electron bombardment energy was 23 eV. The product peaks for C_nH_m are labeled by n, the number of carbon atoms. Arrows indicate masses for $m = n$ (located at $n \times 13$ mass units); thus $m \approx n$ up to $n = 8$ but the most probable m is lower by 1 to 3 units for higher n.

Figure 4. 14 Experimental results from ethane pyrolysis at 1060K. Note the large peaks for C_2H_2 (off the scale) and C_6H_6. L. Shebaro et al.

Chapter 5

Conclusion

Hydrogen production from steam reforming and pyrolysis has been evaluated through thermodynamic equilibrium calculations. Results show benefits and hindrances to producing hydrogen by these processes. A comparable amount of H_2 can be made per mole of fuel by either process as seen in table 5.1; however, pyrolysis requires a higher energy input to bring the reactants to the operating temperature of 1500K. Though steam reforming is both a low temperature and efficient process as illustrated in figure 5.1, it produces by products, namely, CO, that reduces its productivity; this disadvantage is not realized with pyrolysis. Reaction rate of reforming and pyrolysis should now be addressed. A catalyzed reformer or a pyrolyzer can produce H_2 from a fuel molecule in a characteristic time call the residence time. The residence time for steam reform is 0.1 – 0.25s [32] while residence times for pyrolysis is about 10ms [31]. Pyrolysis cost more energy but, can produce hydrogen ten to twenty times faster. Pyrolysis of light hydrocarbons can be considered as a viable option to produce hydrogen.

Table 5. 1 Comparison of hydrogen production from steam reforming and pyrolysis.

	H_2 mass (g)	H_2 mass fraction (%)	Temp (K)
Methanol	6	10	416
Methyl Formate	4	7	411
DME	6	12	424
Methane	3.6	16	1500
Ethane	3	12	1500

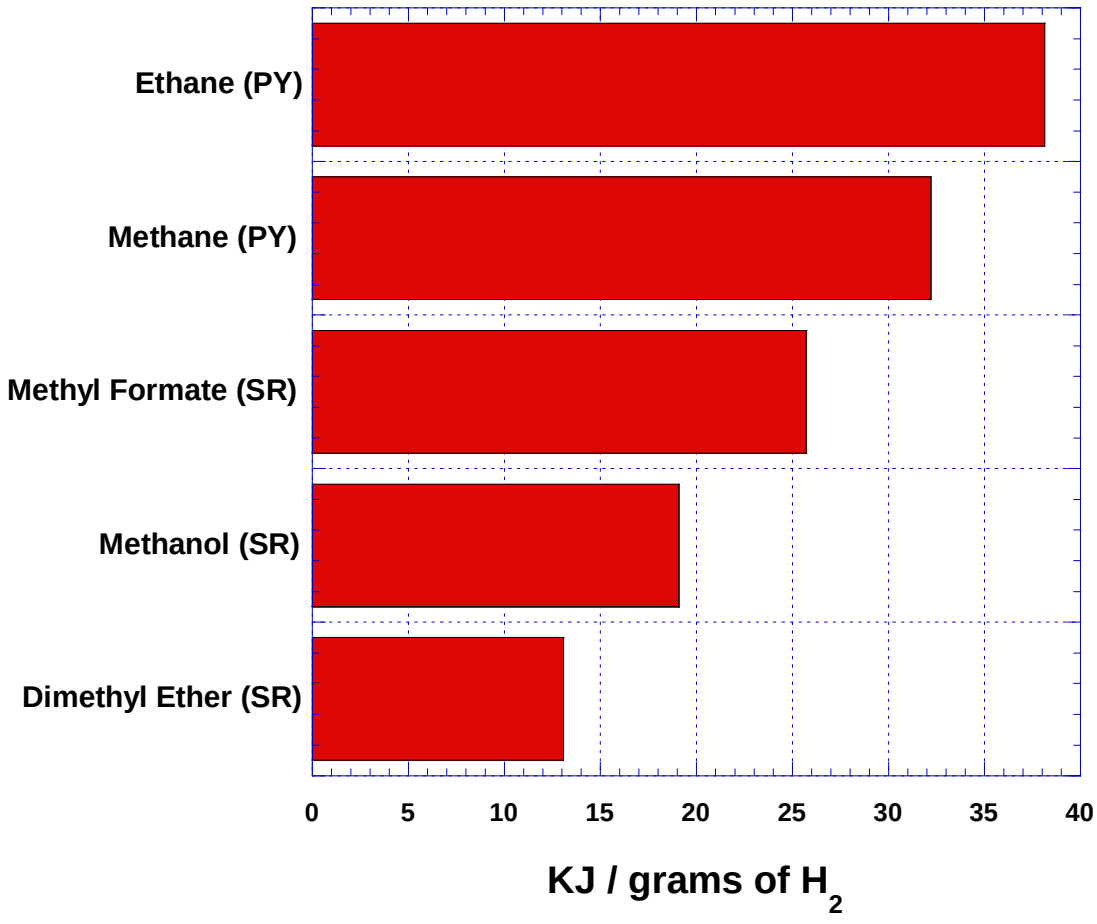

Figure 5. 1 Energy consumption for H_2 production. Although pyrolysis cost the most energy it produces hydrogen ten times faster.

Appendix

The following is the computer algorithm used to compute equilibrium compositions of methanol steam reforming products. Simple modifications can be made to model other fuels. This code makes use of a Numerical Algorithms Group's mathematical algorithm for solving simultaneous non-linear equations. The code is written with FORTRAN 90 syntax.

```
MODULE nlin_sys_ex01_mod
! .. Implicit None Statement ..
IMPLICIT NONE
! .. Intrinsic Functions ..
INTRINSIC KIND
! .. Parameters ..
INTEGER, PARAMETER :: wp = KIND(1.0D0)     !!!!!!!!!!!!!!!!!!!!!!!!!!!!!!!!!!!!!!!!!!!!!
REAL, PARAMETER :: H = 7.0_wp              !    Input # of atoms of Hydrogen    !
REAL, PARAMETER :: O = 3.5_wp              !        Oxygen and Carbon           !
REAL, PARAMETER :: C = 1.0_wp              !!!!!!!!!!!!!!!!!!!!!!!!!!!!!!!!!!!!!!!!!!!!!
CONTAINS
SUBROUTINE fun(x,finish,f_vec,f_jac)
! .. Implicit None Statement ..
```

```
IMPLICIT NONE
! .. Intrinsic Functions ..
INTRINSIC SIZE
! .. Scalar Arguments ..
LOGICAL, INTENT (INOUT) :: finish
! .. Array Arguments ..
REAL (wp), OPTIONAL, INTENT (OUT) :: f_jac(:,:)
REAL (wp), INTENT (OUT) :: f_vec(:)
 REAL (wp), INTENT (IN) :: x(:)
! .. Local Scalars ..
INTEGER :: n
! .. Executable Statements ..
! f_vec( ) is the nominclature from NAG

! Each equation is understood to be (ie. implicitly) set equal to zero by the program

! f_vec(1 - 10) are the equilibrium equations from the litureature esp.

! x(1) is the variable for H2          x(7) is the variable for the sum of x(1) through x(6)
! x(2) is the variable for H2O         x(8) is the Lagrange multiplier for Hydrogern
! x(3) is the variable for CO2         x(9) is the Lagrange multiplier for Carbon
! x(4) is the variable for CO          x(10) is the Lagrange multiplier for Oxygen
! x(5) is the variable for CH3OH (Methanol)
```

! x(6) is the variable for CH3OCHO (Methelformate)

! x(11) is the variable for Temp*Gas constant and f_vec(11) is the coresponding equation

! x(12) is the variable for x(11)*Ln of pressure and f_vec(12) is the coresponding equation

! x(14) is the Ln of pressure in units of bar

```
!!!!!!!!!!!!!!!!!!!!!!!!!!!!!!!!!!!!!!!!!!!!!!!!!!!!!!!!!!!!!!!!!!!!!!!!!!!!!!!!!!!!!!!!!!!!!!!!!!!!!!!
f_vec(1) = x(1) + x(2) + x(3)+ x(4) + x(5) + x(6) - x(7)
f_vec(2) = 2.0_wp*x(1) + 2.0_wp*x(2) + 4.0_wp*x(5) + 4.0_wp*x(6)- H
f_vec(3) = x(3) + x(4) + x(5) + 2.0_wp*x(6) - C
f_vec(4) = x(2) + 2.0_wp*x(3)+ x(4) + x(5) + 2.0_wp*x(6) - O
f_vec(5) = 0.0_wp + 2.0_wp*x(8) + x(12) + x(11) * LOG(x(1)/x(7))
f_vec(6) = -242.85_wp+0.045656_wp*x(13)+4.5e-6_wp*x(13)*x(13) + 2.0_wp*x(8) +
x(10) + x(12) + &       x(11)* LOG(x(2)/x(7))
f_vec(7) = -393.41_wp-0.0035756_wp*x(13)+1.1185e-6_wp*x(13)*x(13) + x(9) +
2.0_wp*x(10) +     &  x(12) + x(11) * LOG(x(3)/x(7))
f_vec(8) = -109.48_wp-0.093234_wp*x(13)+2.4706e-6_wp*x(13)*x(13) + x(9) + x(10)
+ x(12) + x(11) &       * LOG(x(4)/x(7))
f_vec(9) = -205.6_wp+0.13912_wp*x(13)+9.975e-6_wp*x(13)*x(13) + x(9) +
4.0_wp*x(8) + x(10) + &       x(12)+ x(11) * LOG(x(5)/x(7))
f_vec(10)= -351.2_wp+0.17586_wp*x(13)+1.5536e-
5_wp*x(13)*x(13)+2.0_wp*x(9)+4.0_wp*x(8)+2.0_wp*x(10)+&
```

```
x(12)+x(11)*LOG(x(6)/x(7))

f_vec(11) = x(13)*8.31_wp* 1.0E-3_wp-x(11)

f_vec(12) = x(11)*x(14)-x(12)

WRITE (90,'(/1X,A/1(F25.17))') &

        f_vec(1),f_vec(2),f_vec(3),f_vec(4),f_vec(5),f_vec(6),f_vec(7),f_vec(8),f_vec(9),

f_vec(10)

END SUBROUTINE fun

END MODULE nlin_sys_ex01_mod

PROGRAM nag_nlin_sys_ex01

! .. Use Statements ..

USE nag_examples_io, ONLY : nag_std_out

 USE nag_nlin_sys, ONLY : nag_nlin_sys_sol

USE nlin_sys_ex01_mod, ONLY : fun, wp

! .. Implicit None Statement ..

IMPLICIT NONE

! .. Parameters ..

INTEGER, PARAMETER :: n = 14

! .. Local Arrays ..

REAL (wp) :: x(n)

REAL (wp) :: I,J,K,num,PresTemp,pres      ! User defined variables

! .. Executable Statements ..

! Starting values for the initial approximate solution

OPEN (10, file = 'Temp.txt' )                    !store Temperature*Gas constant here
```

```
OPEN (20, file = 'Temp2.txt')                !store Ln of Pressure*Temperature*Gas
constant here
OPEN (30, file = 'Temp3.txt')                !store Temperature here
OPEN (40, file = 'Temp4.txt')                !store Ln of Pressure in units of bar here
OPEN (50, file = 'MeOH_input.txt')           !this is input file
OPEN (70, file = 'MeOH_next.txt')            !this is output for the next file
OPEN (80, file = 'MeOCHO_2.5 steam H(T).txt')   !this is formated output
OPEN (90, file = 'go_figure4.txt')           !this to inspect accuracy of initial guesses
READ (50,*) x(1),x(2),x(3),x(4),x(5),x(6),x(7),x(8),x(9),x(10)
J = 0.0_wp                                   !Ln of pressure in units of bar
DO I = 300.0_wp, 1000.0_wp, 5.0_wp
num = I * 8.31_wp * 1.0E-3_wp
pres = J
PresTemp = pres * num
WRITE (10,*) '', num
WRITE (20,*) '', PresTemp
WRITE (30,*) '', I
WRITE (40,*) '', pres
backspace 10
backspace 20
backspace 30
backspace 40
READ (10,*) x(11)
```

```
READ (20,*) x(12)

READ (30,*) x(13)

READ (40,*) x(14)

CALL nag_nlin_sys_sol(fun,x,user_jac=.FALSE.)

WRITE (70,'(/1X,A/1(F25.17))') '', x

WRITE (80,'(/1X,A/14(F13.7))') '', x

DO K = 0, 14, 1                    !Backspace 14 times. Once for each variable before reading

file

backspace 70

END DO

READ (70,*) x(1),x(2),x(3),x(4),x(5),x(6),x(7),x(8),x(9),x(10)

END DO

END PROGRAM nag_nlin_sys_ex01
```

REFERENCES

[1] R. O. Idem and N.N. Bakhshi, *Chemical Engineering Science*, **51**(14) 3697-3708, 1996

[2] B. A. Pepply et al., *Applied Catalysis A: General*, **179** 21-29, 1999

[3] P. J. de Wild and M. J. F. M. Verhaak., *Catalysis Today*, **60** 3-10, 2000

[4] S. Amad and M. Krumpelt., *Int. J. of Hydrogen Energy*, **26** 291-301, 2001

[5] L. F. Brown., *Int. J. of Hydrogen Energy*, **26** 381-397, 2001

[6] Y. Lwin et al., *Int. J. of Hydrogen Energy*, **25** 47-53, 2000

[7] J.C. Amphlet et at., *Canadian Journal of Chemical Engineering*, **59** 720-727, 1981

[8] USEPA 1994a

[9] T. D. Brock and M. T. Madigan, 1991. Biology of Microorganisms. Prentice Hall Englewood, NJ.

[10] Malcolm Pirnie, Inc. Evaluation of the Fate and Transportation of Methanol in the Environment, American Methanol Institute, 1999

[11] A. Lutz, R. S. Larson, J. O. Keller, *Int. J. of Hydrogen Energy*, **27** 1103-1111, 2002

[12] M. Ahman, *Energy*, **26** 973-989, 2001

[13] R. E. Katofsky, The production of fluid fuels from biomass. Princetion, (NJ): Center for Energy and Environmental Studies, 193

[14] M. Wang,. *J. of Power Sources*, **112** 307-321, 2002

[15] D. W. Oxtoby and N. H. Nachtreb, 1990. Principles of Modern Chemistry. Sanders College Publishing

[16] R. C. Oliver, S. E. Stephanou, R. W. Baier, *Chemical Engineering*, 121-128, 1962

[17] W. B. White, S. M. Johnson, G. B. Dantzig, *J. Chem Phys*, **28**(5) 751-755

[18] E.Y. Garcia and M. A. Laborde, Int. J. Hydrogen Energy, **16**(5) 307-312, 1991

[19] J.J. Mor´e , B. S. Garbow, K. E. Hillstrom, User guide for MINPACK-1 *Technical Report ANL-80-74* Argonne National Laboratory, 1974

[20] J. A. Laurnann and R. M Rotty, J. Geophys. Res. **88**, (1983) 1295

[21] Ilias M. Vardavas and John H. Carver, Planet Space Sci. **33** (1985) 1187

[22] C. D. Dudfeild, R. Chen, P. L. Adcock, *Journal of Power Sources*, **85** 237-244, 2000

[23] Ahmet K Avci et al, *Applied Catalysis A: General*, **216**, 243-256 2001

[24] Chunshan Song, *Catalysis Today,* **77**(1-2),17-49, 2002

[25] Mitsuaki Echigo and Takeshi Tabata, *Applied Catalysis A: General*, **251**(1), 157-166 2003

[26] J. C. Amplett et al, *J. Hydrogen Energy*, **19**(2), 131-137 1994

[27] C. D. Dudfeild, R. Chen, P. L. Adcock, *Journal of Power Sources*, **85** 237-244, 2000

[28] P. Atkins,. Physical Chemistry, Freeman, 1994

[29] C. Gueret, M. Daroux, F. Billaud, *Chemical Engineering Science*, **52**(5), 815-827, 1997

[30] L. Romm, G. A. Somorjai, *Catalysis Letters*, **64**, 85-93, 2000

[31] L. Shebaro, S. R. Bhalotra, D. Herschbach, *J. Phys Chem A*, **101**, 6775-80, 1997

[32] P. Pfeifer et al., Microreaction Technology: Industrial Prospects, Proceedings of the International Conference on Microreaction Technology, 3rd, Frankfurt, 372-382, 1999